

Al-Neelain University

Postgraduate College



**Synthesis and Characterization of
(Ba_(1-x)Mg_xTi_(1-x)Mn_xO₃) Single Perovskite
Oxide**

**A Thesis submitted in partial fulfillment of the Requirements for the Degree
of Master in Physics (Materials Science)**

Prepared by:

Mohammed Awadh Saeed Al-Ameri

Supervisor

Dr: Musbah Hamed Babikier

March – 2018

~~Handwritten signature in red ink~~

جامعة النيلين
كلية الدراسات العليا - مكتب العميد
29 MAR 2018
AL-NEFTALI UNIVERSITY
GRADUATE STUDIES DEAN OFFICE

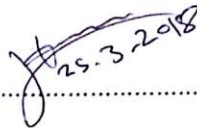
بسم الله الرحمن الرحيم

جامعة النيلين

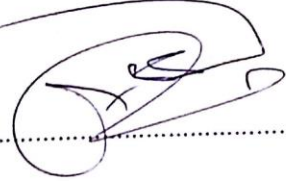
كلية الدراسات العليا

لجنة المناقشة

Dr. Hassan Abdelhalim Abdallah


29.3.2018

Dr. Hassan Hamad Abuelhassan


28/3/2018

Dr. Musbah Hamed Babikier



بسم الله الرحمن الرحيم

الآية

قال الله تعالى :

وَيَسْأَلُونَكَ عَنِ الرُّوحِ قُلِ الرُّوحُ مِنْ أَمْرِ رَبِّي وَمَا أُوتِيتُمْ مِنَ

الْعِلْمِ إِلَّا قَلِيلًا ﴿٨٥﴾

صدق الله العظيم

سورة الإسراء الآية ٨٥

DEDICATION

I dedicate this research to:

My mother and father, who are the sources of happiness in my life.

My brothers and sisters.

My wife and my children, who are the secret of my success and achievement in the study.

My Supervisor Dr. Musbah Hamed Babikier, who is who helped me and gave me support to complete this work.

My classmates, all my teachers and doctors from primary school to graduate college and my friends Youssef Alsabab and Gobran Ali.

Mohammed

ACKNOWLEDGEMENT

First, I thank Allah, who gives me the opportunity and strength to carry out this work. My greatest thanks are to my parents who bestowed ability and strength in me to complete this work. I would like to express my gratitude to my supervisor **Dr. Musbah Hamed Babikier** for guidance and support throughout my thesis work. He has been a constant source of inspiration to me throughout the period of this project. I consider myself extremely fortunate for having the opportunity to learn and work under his supervision over the entire period.

I would also take this opportunity to express my gratitude and my thanks to any one for his help and support for me .I would also take these thanks for staff of material science lab and laser lab in Al-Neelain University (Prof.Yousif Sulfab Ahmed , Dr. Abdel-Sakhi , Mr. Idris , Mr. Gobran Ali , and Mr. Yousief Alsabah) for their help, inspiration, and moral support .I take this opportunity to express my profound sense of gratitude and respect to my colleagues, and all those who helped me through the duration of this project work.

ABSTRACT

Five samples of single perovskite oxides of formula $Ba_{(1-x)}Mg_xTi_{(1-x)}Mn_xO_3$ where $x = 0.01, 0.2, 0.03, 0.04, \text{ and } 0.05$ were synthesized using solid state reaction method, and the samples were calcinated at $1200^\circ C$. All samples were investigated by spectroscopy techniques such as, X-ray diffraction (XRD), Fourier Transform Infrared Spectroscopy (FTIR), and Ultraviolet Visible Spectroscopy (UV-visible), and. The XRD results confirmed that the five samples had a cubic phase, and the average of lattice constants, and the average of grain sizes increased with dopant from sample 1 to sample 4 ($4.0512A^\circ, 4.2086A^\circ, 5.087A^\circ, \text{ and } 5.1955A^\circ$), ($29.3nm, 32.4nm, 36.15 nm, \text{ and } 37.98 nm$) respectively, and they decreased with contents of Mg and Mn in sample 5 ($5.0184A^\circ$), ($37.5 nm$) respectively. Also the intensity increased with dopant of Mg and Mn in samples 1, 2, 3, and 5, and it decreased in sample 4. The FTIR spectroscopy results showed that the transmittance of the five samples decreased with contents of Mg and Mn at $BaTiO_3$. On other hand, the Ultraviolet Visible Spectroscopy (UV) proved that the absorption of five samples have been increased with increasing of Mg and Mn doping in $BaTiO_3$, and the optical band gap energy increased with Mg and Mn contents at $BaTiO_3$ ($3.18, 4.31, 4.35, 4.39, \text{ and } 4.43 eV$), which results in decreasing of reflective indexes ($2.31, 2.10, 2.09, 2.089, \text{ and } 2.083$) respectively. These results were attributed to the doping of elements in A and B sites.

المستخلص

تم تحضير عينات من أكاسيد البروفسكايت الأحادية $Ba_{(1-x)}Mg_xTi_{(1-x)}Mn_xO_3$ حيث أن $x = 0.01, 0.02, 0.03, 0.04, \text{ and } 0.05$ وتمت معالجتها حرارياً باستخدام الطريقة التقليدية وهي تفاعل الحالة الصلبة وحيث أن جميع العينات تم تكليسها عند 1200°C درجة مئوية. جميع العينات تم تحليلها بواسطة تقنيات الطيف المختلفة مثل مطياف حيود الأشعة السينية و مطياف الأشعة تحت الحمراء و المطياف الضوئي للأشعة فوق البنفسجية. تم التأكد بواسطة مطياف حيود الأشعة أكد أن جميع العينات لها طور كيميائي مكعب و أن ثابت الشبكة وحجم الحبيبات تزداد من العينة الأولى إلى العينة الرابعة (5.0184Å ، 5.0184Å) على الترتيب وكما أن ثابت الشبكة وحجم الحبيبات تقل عند العينة الخامسة (5.0184Å)، (37.5nm) على الترتيب. كما أن جهاز قياس طيف الأشعة تحت الحمراء أثبت أن النفاذية تقل بزيادة نسبة تشويب عنصري المغنيسيوم والمنجنيز في مركب تيتانات الباريوم. ومن ناحية أخرى المطياف الضوئي للأشعة فوق البنفسجية أكد أن الامتصاصية للخمس العينات تزداد بزيادة نسب التشويب لعنصري المغنيسيوم والمنجنيز، وتم حساب فجوة الطاقة ووجدت أنها تزداد بزيادة نسبة التشويب (3.18eV ، 3.18eV ، 4.35eV ، 4.39eV ، 4.43eV بوحدة الإلكترون فولت) على الترتيب. وكذلك فإن معامل الانكسار يقل بزيادة نسبة التشويب للعنصرين المذكورين أعلاه (2.31 ، 2.10 ، 2.09 ، 2.089 ، 2.083). جميع النتائج تعود إلى تشويب عنصري المغنيسيوم والمنجنيز في تيتانات الباريوم.

Contents	
الآية	I
DEDICATION	ii
ACKNOWLEDGEMENTS	iii
ABSTRACT	iv
المستخلص	v
TABLE OF CONTENTS	vi
LIST OF FIGURS	viii
LIST OF TABLES	ix
LIST OF SYMBOLS	x

Chapter One - Introduction	
1.1. Historical Background of Single Preovskite Oxide	1
1.2. Objectives	2
1.3 . Outlines	2

Chapter Two - Theoretical Background	
2.1. Literature review	3
2.2. Preovskite Structure	11
2. 3 . Properties of Barium Titanate Ceramics	12
2.3.1. Dielectric Properties	12
2.3.2 . Electrostrictive Vibration	12
2.3.3. Electrostrictive and Piezoelectric Phenomena	13
2.3.4. Electronic and Magnetic Properties of Barium Titanate	13
2.3.5 . Structural Properties of Barium Titanate	14
2.3.6. Optical properties of Barium Titanate	14

Chapter Three - Experimental Work	
3.1. solid satet reaction method	15
3.2 . Fabrication	15
3.3. Characterization Techniques	20
3.3.1. Prepration samples for XRD spectroscopy	20
3.3.2. Principle of X-ray Diffraction Spectroscopy	20
3.3.3. Prepration Samples for FTIR Spectroscopy	21
3.3.5. Prepration samples for Uv-visible spectroscopy	22
3.3.6. Principle of UV-visible Spectroscopy	23
3.3.7. The Beer-Lambert Law	23

Chapter Four - Results and Discussion	
4.1. XRD analysis	24
4.2. FTIR analysis	29
4.3. UV-Visible	34
4.4. Calculation of band gap Energy	35
4.5 .Calculation of Refractive Index	36

Chapter Five - Conclusion and Recommendations	
5.1. Conclusion	38
5.2 . Recommendations	38
5.3. References	39

list of Figures

figures	Item	Page No
2.1	structure of single perovskite oxide (octahedra)	11
2.2	structure of single perovskite oxide (cubic)	11
2.3a	Cubic structure of $BaTiO_3$	14
2.3b	Tetragonal structure of $BaTiO_3$	14
3.1	KERN electronic balance Capacity 120 g Readbility:0.1mg	16
3.2	A great mortar equipment	18
3.3	Laboratory oven (lab-tech), volt 230, watts 500Serial No: 14125, size: 14x14, Manufacturing in India	18
3.4	Five Crucibles	19
3.5	CARBOLITE –CWF 1200° C Serial No: 20-302426 Manufacturing in England	19
3.6	Phelps XRD, Serial number: 943003040601, Manufactured in Holland	20
3.7	Satellite FTIR ... Serial N0 20010102 Voltage. +5/+15/-15 VDC... Manufactured in U.S.A	21
3.8	schematic representation of the electromagnetic spectrum	22
3.9	UV mini- 1240 CE... Serial No A10934081718 Sm 220- 240 V- 50 / 60HZ – 160 VA Manufactured in Germany	22
4.1	XRD combined for all five samples.	24
4.2	FTIR spectrum of combined for all five samples	29
4.3	UV- visible absorption combined for all five samples	34

4.4	optical band gap energy combined for all five samples	35
-----	---	----

List of Tables

figures	Item	Page No
3.1	the weights of each sample is 1 gm	17
3.2	the weight of each sample is 2gm	17
4.1	the XRD results of $Ba_{0.99}Mg_{0.01}Ti_{0.99}Mn_{0.01}O_3$ single perovskite oxide	25
4.2	the XRD results of $Ba_{0.98}Mg_{0.02}Ti_{0.98}Mn_{0.02}O_3$ single perovskite oxide	25
4.3	the XRD results of $Ba_{0.97}Mg_{0.03}Ti_{0.97}Mn_{0.02}O_3$ single perovskite oxide	26
4.4	the XRD results of $Ba_{0.96}Mg_{0.04}Ti_{0.96}Mn_{0.04}O_3$ single perovskite oxide	26
4.5	the XRD results of $Ba_{0.95}Mg_{0.05}Ti_{0.95}Mn_{0.05}O_3$ single perovskite oxide	27
4.6	comparing between the average of lattice constants and grain sizes of the five samples	28
4.7	the identical and shifted FTIR absorption bonds for all five samples	33
4.8	the values of refractive index of five samples	36
4.9	comparing between Uv-Visible results	37

List of symbols

symbol	Item
ABO_3, ABX_3	The formula of single preovskite structure
$BaTiO_3$	Bruim titanate
$CaTiO_3$	Clacuim titante
FTIR	Fourier Transform Infrared Spectroscopy
UV-visible	Ultraviolet Visible Spectroscopy
XRD	X-ray diffraction
a.u	Arbitrary unit
x,y	Moular fractions
ϵ'	The maximum value of dielectric constant
SEM	Scanning electron microscope

KHZ, MHZ	Units of frequency
a,b,c	lattice parameters
α, β, γ	Angles of chemical phase
EXAFS	Extended X-ray absorption fine structure
E	Intenial energy
EDX	Energy –dispersive X-ray spectroscopy
CW	Cornelius Warren law
dc	Direct current
ϵ_{\max}	Maximum value of dielectric
λ	Wavelength
E	Energy
h	Planck constant
ν	Frequency
C	Speed of light
T	Transmittance
I	Intensity of transmitted light
I_0	Intensity of incident light
ϵ_{λ}	Extinction coefficient
d	Path length
C	Concentration
eV	Electron volt is unit of enegy
h,k,l	Miller coefficients
d	Inter-planar spacing
θ	Scatteing angle of electron
P	Power

E	Young's modulus
ρ_1	Density of liquid
V_1	sound velocity of the liquid
ρ_o	Density of velocity of barium titanate ceramics
V_o	Sound velocity of barium titanate ceramics
$(\Delta p)^2$	The maximum of stress
n_o	Reflective index of pure barium titanate
N	Number of atoms
d_{33}	piezoelectric coefficient
σ	Poisson's ratio
ρ	The density
T_c	Currie point temperature
(γ)	phase transition
gm	Unit of mass

CHAPTER ONE

Introduction

1.1. Historical Background of Single Perovskite Oxide:

Single Perovskite oxide is a mineral of formula ABX_3 , such as $BaTiO_3$ and $CaTiO_3$ where Ba or Ca represents A site, and Ti denotes to B site. This type of mineral was discovered in 1839 by the Prussian mineralogist Gustav Rose in mineral deposits in the Ural Mountains. The first work of preparation the Perovskite was done by V.M Goldschmidt. The mineral perovskite can be formed at a high temperature which embodies ideal structure for it, and the basic building block consists of a single cubic (Bhalla et al., 2000).

Perovskite system contains two main classifications halide perovskites and inorganic oxide perovskites. The first classification divided to organo-metal halide perovskites and alkali-halide perovskites. The second classification contains doped perovskites and intrinsic perovskites (Bhalla et al., 2000).

The natural crystal of single perovskite has many attractive physical properties such as mechanical, optical, electrical, and structural properties. The mechanical properties include hardness within the range (5.5-6), and density about (4000-4300) kg/m^3 . On the other hand, the optical properties like color can be changed from brown to black to gray, from brown to orange to yellow to white, and refractive index of pure single perovskite is 2.38. The structural properties confirmed that the crystal structure of this material thought to be cubic, orthorhombic, and tetragonal. Also, the electrical properties showed that the perovskite material has ferroelectric properties at a high temperature (Tilley, 2016, Vijatović et al., 2008).

Perovskite material can be used in many applications such as capacitors, multilayer capacitors, and solar cell because it chemically and mechanically is very stable, and it can be prepared easily as polycrystalline samples (Tilley, 2016, Vijatović et al., 2008).

Barium titanate is the one of perovskite family which it has a chemical formula $BaTiO_3$, and it was discovered by Von Hippel, Wul, and Golman during the Second World War in 1941 and 1944 in the United States, Russian, and Japan. A lot of researchers have been studied the

properties of barium titanate because it has good physical properties such as ferroelectric ceramics properties. It can be prepared by many methods like solid state reaction, sol gel ,and hydrothermal (Tanaka, 1954).

The $BaTiO_3$ is a prototypical ferroelectric material with a characteristic tetragonal distortion of the cubic perovskite structure. The ferroelectric distortion is facilitated by the large size of the Ba cation. Replacement of Ba by any single or divalent element can be led to a perovskite with cubic or tetragonal structures. The origin of the ferroelectric property is a displacement of the Ti atoms by each quadratic or parietal equivalence element, and this effect is very sensitive to increased or decreased the lattice parameters (Wahl et al., 2008) .

1.2. Objectives:

- ❖ The first aim of the present work is to synthesis a new material of single Preovskite Oxide by using one of perovskite family $BaTiO_3$,which will doped by Mg in A site and Mn in B site of $Ba_{(1-x)}Mg_xTi_{(1-x)}Mn_xO_3$ where molar fraction (x) =0.01, 0.02 , 0.03 , 0.04 , 0.05 via solid state reaction method.
- ❖ The second aim is to study the optical properties and calculate the band gap energy and refractive index.
- ❖ The third aim is studying the structural properties of the new material of single Preovskite Oxide.

1.3. Outlines of this thesis:

This research contains five chapters. Chapter one presents an introduction, which includes brief historical background of the single perovskite oxide, barium titanate. The second chapter illustrates the theoretical background of the research topic and general literature review. The experimental work will be shown in chapter three in details. Chapter four presents discussion of the obtained results. The conclusion and recommendation will be clarified in chapter five.

CHAPTER TWO

Theoretical Background Perovskite

2.1. Literature Review

Titanate compounds like barium titanate ($BaTiO_3$) have been extensively studied as crystalline samples during last decades because of its excellent ferroelectric properties, and they have very good stability of its chemical and mechanical perovskite structure. Barium titanate $BaTiO_3$ is the most perfect material for many applications such as dielectric capacitors and ceramics with positive temperature coefficient resistance as documented by (Kadira et al., 2016, Khare and Chauhan, 2015).

Many researchers have been prepared $BaTiO_3$ which was doped in A site of this compound, and they have been studied some physical properties of doped barium titanate such as, optical, structural, and electrical properties. Also, they have been found attractive results as shown at below:

The electrical, optical and structural properties of Ag- doped $BaTiO_3$ were studied by Hao et al., 2011. The lowest point of resistivity was $5.644\Omega.m$, also, the characteristic of absorption frequencies found at the chemical bonds such as, O-H, and Ti-O. The XRD results showed that the patterns changed slightly their positions after doping and after calcinations. Also, the particle size of the samples was 11.81 nm, 20.31 nm and 18.29 nm respectively (Hao et al., 2011).

Other research was prepared $Ba_{1-x}Ni_xTiO_3$ by Bisen et al., 2016, and they were discussed the structural, optical, and electrical properties of samples. The XRD results confirmed that the samples have a tetragonal phase with space group P4mm. The characteristic of absorption frequencies found at the chemical bonds such as, O-H, C-H, and C=O. The electric studies indicated that the dielectric constant increased from 1 Hz to 10^5 Hz (Bisen et al., 2016).

The gels and powders of $(pb_{1-x},Ba_x)TiO_3$ were prepared by Zhu et al., 2011, and they were studied some physical properties of this compounds. The FTIR frequencies of gels showed some chemical bonds such as, Ti-O-C, Ba-O, Ti-O, Ti-C-O. The Raman spectra indicated to

another chemical bonds like C–O, Ti–O. The FTIR results of powders found some organic C–H, , and C–O. The XRD technique showed that the samples have a phase transformed from the cubic phase to the pseudo-cubic phase. The average of particle sizes were approximately (40-80 nm) . (Zhu et al., 2011).

Another project was synthesized Al and Mg co-doped of $BaTiO_3$ by Khongnakhon and Jongprateep, and they were studied the structural and electrical properties of samples. The XRD results showed that the average of particle sizes increased with dopant of Al and Mg (Khongnakhon and Jongprateep, 2013).

The $Ba_{1-x}La_xTi_{1-x/4}O_3$ was prepared by Morrison et al., and they were studied the structural and electrical characteristics of lanthanum-doped barium titanate ceramics. The structural results showed that the samples can be changed from tetragonal to cubic phase or from orthorhombic to tetragonal phase. The electrical results showed that the value of the maximum permittivity at the tetragonal/cubic phase transition in ceramic samples increased doping ratio (Morrison et al., 1999).

The ceramics samples of calcium-doped barium titanate were prepared by Alaraj et al., 2017, and they were displayed the electrical properties of $Ba_{1-x}Ca_xTiO_3$. The electrical properties of ceramic samples showed that the Currie point temperature (T_c) changed from $120^\circ C$ to $150^\circ C$, and the dielectric constant decreased by increasing of the calcium-added ratio (Alaraj et al., 2017) . Other studying was prepared $Ba_{1-x}Ca_xTiO_3$ by Kadira et al., 2016, and they were discussed the electrical and structural properties of calcium doped barium titanate ceramics. The X-ray diffraction showed that the powders of $Ba_{1-x}Ca_xTiO_3$ was crystallize in a concentrations of the $BaTiO_3$, and the dielectric study of $Ba_{1-x}Ca_xTiO_3$ increased with dopant (Kadira et al., 2016) .

Another single preovskite oxide was synthesized $Ba_{1-x}Gd_xTi_{1-x/4}O_3$ by Hernández Lara et al., 2017 ,and they were studied structural and electrical properties of this new preovskite structure. The XRD results confirmed that the crystal phase of the obtained particles was predominately tetragonal phase, and the electrical results showed that the maximum permittivity values were recorded for the samples with $x = 0.001, 0.005, \text{ and } 0.1$ (Hernández Lara et al., 2017) .

Furthermore, Miclea et al., 2006 were prepared the uranium doped barium titanate, and they were discussed the electrical and structural properties of $Ba_{1-x}U_xTiO_3$. The electrical results showed that the resistivity decreased with doping, and it increased to $10^7 \Omega.cm$. Also, this study confirmed that the dielectric constant increased with increasing of U-content. The XRD results confirmed that the samples have perovskite structure (Miclea et al., 2006).

On the other hand, some researchers have been prepared $BaTiO_3$, which was doped in B site of barium titanate single perovskite oxide, and they studied the optical, structural, and electrical properties of these material. Also, they have been found good results as shown at below:

The Mg doped barium titanate ceramics samples were prepared by Cai et al., 2011, and they were displayed the structural and electrical properties of the samples. The XRD results indicated that the patterns of barium titanate ceramics with different MgO contents. First, the patterns were virtually the same and showed only a single phase structure, and the diffraction peaks of samples are shifted to the higher angle side with increasing the Mg content. The dielectric properties confirmed that the temperature dependence of the dielectric constant and the dielectric loss of the pure and Mg doped ceramics increased with increasing of the frequency. The SEM micrographs of pure and Mg doped ceramics near $60\mu m, 65\mu m, 55\mu m, and 5\mu m$ with increasing of MgO content (Cai et al., 2011).

The ceramics samples of tin-doped barium titanate were prepared by Alaraj et al., 2017, and they were studied the electrical properties of $BaTi_{1-x}Sn_xO_3$. The electrical properties of the samples showed that the maximum value of the dielectric constant up to $\epsilon' = 6568$, and the Curie constant decreased with increasing ratios of tin added to the ceramic samples. Also, the phase transition (γ) for tin-doped barium titanate was the first type with $\gamma = 1.07$, and the maximum value of transition degree $\gamma = 1.64$ at the sample $x = 0.15$ (Alaraj et al., 2017).

Other experimental work was prepared of zirconium doped barium titanate perovskite $Ba(Ti_{1-x}Zr_x)O_3$ by Choudhury et al., 2008, and they were studied some physical properties of these materials. The dielectric showed that the dielectric constant decreased with increasing of frequency, and the resistivity value was $10^3 \Omega.m$, and the grain size of the samples decreased. Also, Dielectric constant of pure $BaTiO_3$ bulk samples showed that the maximum value of about 1000 when grain size was around $1.238\mu m$ (Choudhury et al., 2008).

The Si-doped barium titanate nanopowders were prepared by Langhammer et al., 2009, and they were studied the characterization of the new preovskite materials. The XRD results indicated that the powders were nanopowders and they were all cubic $BaTiO_3$ phase. The electrical results showed that the dielectric properties of the samples have been decreased. (Langhammer et al., 2009).

On the other hand, a lot of researchers have been prepared $BaTiO_3$ which doped in A and B sites (co-doped) of the same compound, and they were studied physical properties like optical, structural, and electrical properties as shown at below:

Badapanda et al., 2016 were prepared pure and Dy- doped of $Ba_{1-x}Dy_{2x/3}Ti_{0.75}Zr_{0.25}O_3$, and they were studied some physical properties such as, the structural and optical properties of the new samples. The XRD results showed that all samples have a single cubic phase structure, and the lattice parameter and cell volume decrease with Dy content. On the other hand, the optical band gap obtained from Uv-visible decrease with Dy doping may be due to creation of oxygen vacancies. Also, The characteristic of absorption frequencies found at the chemical bonds such as , (Ti-O) and (Zr-O) (Badapanda et al., 2016).

Other work was synthesized iron-doped barium strontium titanate $Ba_{0.7}Sr_{0.3}Fe_xTi_{1-x}O_3$ by Kaur et al., 2016, and they were discussed the structural and optical properties of the samples. The XRD results confirmed the samples have tetragonal and cubic structure. The characteristic of absorption frequencies found at the chemical bonds such as, Ti-O , Ti-O-Ti (Kaur et al., 2016).

The lanthanum-magnesium and lanthanum-manganese donor-acceptor barium titanate semiconducting were prepared by Ting et al., 1990, and they were studied the electrical properties of the samples. The electrical properties confirmed that the resistivity of La-doped near $10^{10}\Omega.cm$. Also this study showed that the surface charge density increased near the grain boundaries and contributed to the higher room temperature resistivity. In addition, Acceptor dopant Mn exists as the divalency ions when substituted on the Ti site of $BaTiO_3$ preovskite in the bulk grain region (Ting et al., 1990) .

Other experimental work was prepared $(Ba_{0.9}Mg_{0.1})(Zr_xTi_{1-x})O_3$ ceramics by Gattu et al., 2015, and they were studied the effect of Zr on structural and dielectric properties of the new samples. The XRD results indicated that the samples had cubic and tetragonal phases. On the

other hand ,the SEM micrographs found that the average grain sizes increased with dopant .The dielectric properties confirmed that the dielectric constant increased gradually to a maximum with increasing and decreased again with doping ratio . The maximum dielectric constant is 373, 323, and 180 respectively (Gattu et al., 2015) .

Furthermore, Parkash et al., 2007 were synthesized ($Ba_{1-x}La_xTi_{1-x}Mn_xO_3$), and they were discussed the structural and electrical properties of the samples. The XRD results showed that the samples have been changed from tetragonal, cubic, and orthorhombic to rhombohedral phases. The electrical properties proved that the Curie temperature decrease with increasing of concentration of lanthanum and manganese. The dielectric constant at a cubic to tetragonal transition temperature increased with increasing of x concentrations (Parkash et al., 2007) .

The donor doped barium titanate were synthesized by Stojanović et al., 2004, and they were discussed the structure of barium titanate doped with Nb^{5+} and Y^{3+} . The crystal structure of Nb doped barium titanate showed smaller tetragonality, and the effect of dopants on the change of tetragonality is more expressed in barium titanate doped with niobium than yttrium. Finally, the dielectric behavior of doped barium titanate is in agreement with the presence of the tetragonal structure observed by XRD, and the influence of dopants as well as powder processing is rather significant (Stojanović et al., 2004) .

The $BaTiO_3$ were doped with both Fe^{3+} and Ni^{2+} ions by Aal et al., 2014, and they were discussed the optical and structural of this perovskite compound. The X-ray diffraction showed that the pure and doped $BaTiO_3$ has a tetragonal phase. The characteristic of absorption frequencies found at the chemical bonds such as, O-H ,O-H stretching (Aal et al., 2014) .

Also, Das et al., 2012 were prepared ($Ba_{1-x}Zn_xTi_{1-x}Mn_xO_3$), and they were discussed some physical properties of these new compounds. The XRD results indicated that the chemical phase of samples can be changed from tetragonal to hexagonal phases of doped $BaTiO_3$ ceramics. (Das et al., 2012) .

In addition, Langhammer et al., 1999 were studied the influence of strontium on manganese -doped barium titanate ceramics. The XRD results indicated that the chemical phase of samples was tetragonal (Langhammer et al., 1999).

Other project was prepared Mg-doped barium strontium titanate ceramics by Su and Button, 2004, and they have been studied the microstructure and the dielectric properties of these new compounds (Su and Button, 2004) .

The effect of sintering atmospheres on the microstructure and dielectric properties of Yb/Mg co-doped $BaTiO_3$ ceramics was investigated by Wang et al., 2005. The results showed that the effect of Yb/Mg co-doping on the microstructure and dielectric properties of $BaTiO_3$ ceramics fired under oxidizing, reducing and annealed conditions was investigated. The reducing atmospheres suppressed the solubilities of the acceptor ions; as a result, a second phase of $Yb_2Ti_2O_7$ was detected in the annealed and reducing-fired samples while no second phase was found in the air-fired one (Wang et al., 2005).

Otherwise, Wang et al., 2006 were investigated the dielectric properties of $BaTiO_3$ co-doped with Ni and Nb, and they were discussed the structural and electrical properties of the samples. The XRD analyses proved that the $BaTiO_3$ ceramics has pseudo-cubic structures . The Experiments proved that the incorporation of a proper content of Nb in Ni-doped $BaTiO_3$ can controlled the grain growth, and reduced the dielectric constants. As a result, these new material can be used at many applications such as capacitors (Wang et al., 2006) .

Another elements were doped at $BaTiO_3$ like Y-Al-Ga-Si by Wang et al., 2014, and they were displayed the dielectric and microstructure properties of Y-Al-Ga-Si Co-doped barium titanate ceramics. This study showed that the Y-Al-Ga-Si co-doped barium titanate ceramics have been prepared, and the microstructures, surface morphology, and dielectric properties have been investigated by XRD and SEM analyzer, respectively. Y^{3+} entered into the lattice of $BaTiO_3$, replaced A-sites and B-sites, suppressed grain growth effectively, and made crystal structure has been changed from tetragonal to pseudo-cubic, which reduced dielectric loss and lowered the Curie peak. (Wang et al., 2014).

Another project was prepared of $Ba_{1-x}Ca_xTi_{0.95}Zr_{0.05}O_3$ ceramics by Li et al., 2010, and they were discussed the structural and electrical properties of these compounds. The XRD results showed that the samples had orthorhombic and tetragonal phase. The electrical results proved that the high Curie temperature of $110^\circ C$. (Li et al., 2010).

About highly transparent barium titanate nanothin films for this type was investigated by Ashiri and Helisaie,. The characteristic of absorption frequencies found at the chemical bonds such as, O-H, C-H , C-O ,Ti-O , Ti-O-Ti (Ashiri and Helisaie, 2011).

Eswaramoorthi et al., 2015 were prepared Ga-doped $Ba_{0.6}Sr_{0.4}TiO_3$, and they were discussed the structural, optical and electrical properties of this new perovskite materials. The XRD analysis indicated that the crystallite size decreases with increasing of dopant concentration. SEM analysis proved that the surface smoothness improved with dopant concentration. The EDX analysis confirmed the presence of gallium in the doped material. The dielectric constant and dielectric loss decreased with dopant concentration. The UV-Vis transmission spectrum analysis showed that the transmittance and the refractive index of the film decreased with dopant concentration. The optical band gap of the film increased with dopant concentration (Eswaramoorthi et al., 2015).

The $Ba_{1-3x}La_{2x}Ti_{1-3x}Al_{4x}O_3$ was investigated by Bobade et al., 2005, and they were discussed the structural and electrical properties of the samples. The XRD results showed that the samples have been a tetragonal phase with group space $P4/mm$. The the dielectric can be enhanced by the increasing of the Curie temperature . (Bobade et al., 2005).

The enhanced of Piezoelectric Properties of $Ba_{1-x}Ca_xTi_{0.92}Sn_{0.08}O_3$ was prepared by Zhu et al., 2013, and they were discussed the structural and optical properties of the samples . The XRD results showed that the chemical phase of samples changed from orthorhombic to a tetragonal phase. A high piezoelectric coefficient d_{33} up to 568 PC/N was obtained at x = 0.05 mol, and dielectric constant ϵ_r , reach 47.7%, 1013 pm/V, and 23000, respectively. (Zhu et al., 2013) .

The pure and doped $BaTiO_3$ with some oxides was prepared by many researches, which doped with some oxides and some elements, and they were discussed the some physical properties of the new single preovskite materials as shown at below:

Mohamed and Dughaish, 2012 were prepared $(BaTiO_3)_{1-x}(CeO_2)_x$, and they were studied the optical and structural . The characteristic of absorption frequencies found at the chemical bonds such as, O-H , Ti-O. The XRD showed that the undoped barium had a tetragonal phase. The grain size at the peak 10.55° Ti-O was 44nm, and it was found be near

44nm .At $x=5.7\%$. Also, the grain sizes calculated for the samples with $x=1\%$ and 3% around the 17.25° were found to be 31 nm and 28 nm respectively (Mohamed and Dughaish, 2012).

Also, the group of Sengodan et al., 2012 was prepared $BaTiO_3$ nanoparticles, and they were studied the characterization of this compound. The characteristic of absorption frequencies found at the chemical bonds such as ,O-H and Ti-O (Sengodan et al., 2012).

Another experimental work was synthesized the europium-doped barium titanate nanocrystallites by García-Hernández et al., 2013, and they were studied characterization of these new compounds. The characteristic of absorption frequencies found at the chemical bonds such as, C-O ,Ti-O (García-Hernández et al., 2013).

Other test was prepared nano- $BaTiO_3$ powder by Emre et al.,2014 using by , and they were discussed the characterization of this new material .The X-ray diffraction analysis confirmed that the samples had a cubic phases at room temperature. The SEM results revealed that the morphologies and the particle sizes of the synthesized $BaTiO_3$ was 18.97 nm. The characteristic of absorption frequencies found at the chemical bonds such as, OH, C-O ,C-H (Emre et al., 2014).

Another work was prepared pure and cerium doped barium titanate by Yasmin et al., 2011, and they were studied the structural and dielectric properties cerium Ce- doped $BaTiO_3$. The x-ray diffraction results showed mostly the lattice parameter decreased with the addition of Ce. The electrical properties showed that the dielectric constant showed decreased with an increasing in dopant content. Also, the resistivity decreased in the lower frequency in the range (1-100 kHz), and it remained constant in a high frequency range. In addition, the direct current (dc) density-voltage characteristics of the samples confirmed the ohmic behavior for both the pure and Ce-doped $BaTiO_3$ (Yasmin et al., 2011) .

Furthermore, the nanosized powders and ceramics of Co-doped $BaTiO_3$ were investigated by Bin Cui et al., 2006 via sol–gel process when they mixed all of material together. The characteristic of absorption frequencies found at the chemical bonds such as, O-H ,C-O , Ba-O, and Ti-O. The XRD results showed that there is a cubic structure of $BaTiO_3$. The SEM micrographs of the free surfaces of ceramics confirmed that average grain size of these ceramics was 6.0 nm. Curie temperature of Co-doped $BaTiO_3$ ceramic is shifted to a lower temperature

105° C . The relative dielectric constant at Curie temperature of Co-doped $BaTiO_3$ is higher than the undoped sample. With the increase of Co concentration, the maximum value of dielectric (ϵ_{max}) firstly increased and then decreased (Cui et al., 2006).

2.2. Perovskite Structure:

The perovskite structure oxides that have a chemical formula ABX_3 , where “A” and “B” are cations and “X” is an anion. The “A” and “B” cations can have a variety of charges. In general, the crystal structure is a primitive cubic where the A- larger cation in the corner, but the B-smaller cation in the middle of the cubic, where the anion commonly is an oxygen atom, where it is in the center of the face edge. A is a monovalent, divalent or trivalent metal and B is a pentavalent, tetravalent or trivalent element, respectively. The structure type can be determined by geometrical packing of ions in the lattice, where the perovskite structure can be considered as a three-dimensional framework of BO_6 (octahedra) as shown at figure 2.1, but it can also be regarded as a cubic close packed arrangement of A and O ions, with the B ions filling the interstitial positions as displayed in figure 2.2. The unit cell of the cubic perovskite type lattice can be detected that the coordination number of cation A is 12 and for cation B is 6 (Vijatović et al., 2008).

The perovskite family includes not only compounds with an ideal cubic perovskite lattice, but also all compounds with structures which can be derived from the ideal one by a small lattice distortions or omission of some atoms (Vijatović et al., 2008) .

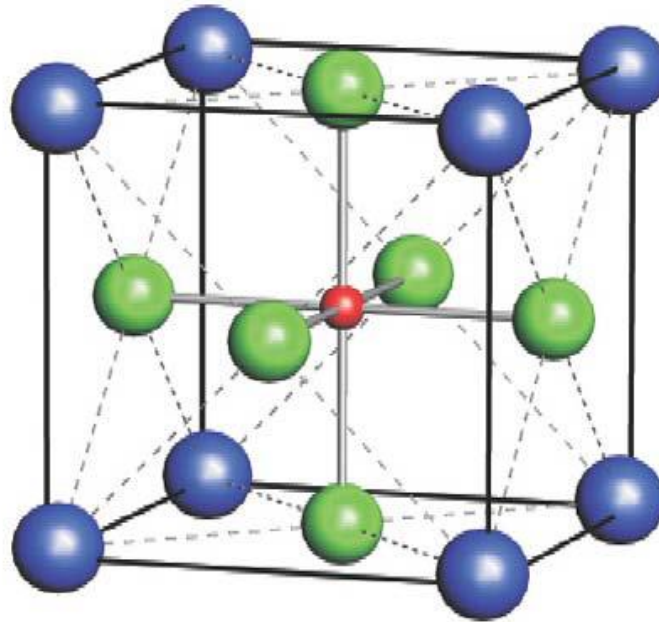


Figure (2.1) structure of single perovskite oxide (octahedra) (Vijatović et al., 2008) .

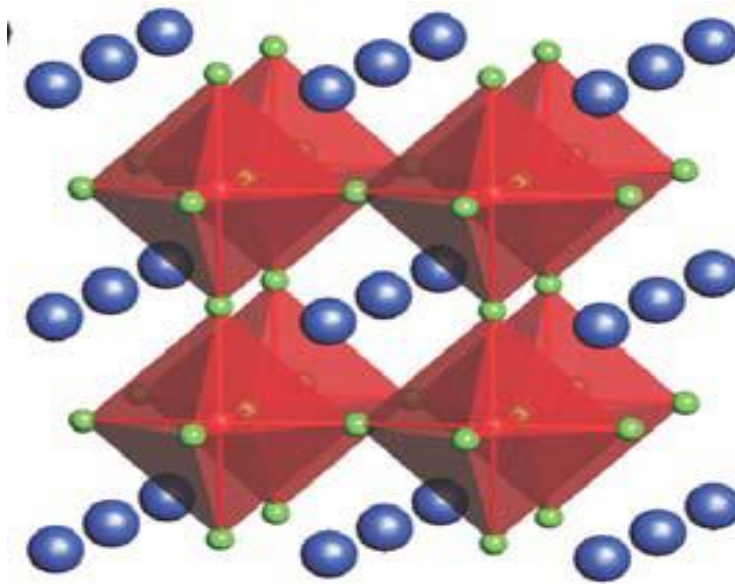


Figure (2.2) structure of single perovskite oxide (cubic) (Vijatović et al., 2008) .

2.3. Properties of Barium Titanate Ceramics:

2.3.1. Dielectric Properties:

The Dielectric constant of pure barium titanate ceramics has a value of (1500- 2000) at room temperature and reaches to (6000-10000) at Curie point near $120^{\circ}C$. They have ferroelectricity at temperatures below Curie point but lose it beyond the point. Therefore, the dielectric loss suddenly drops at temperatures near Curie point, beyond which the loss is generally small. It is also recognized that the Curie-Weiss law holds good between the dielectric constant beyond Curie point and the temperature. The dielectric constant and dielectric loss of barium titanate ceramics are greatly affected by the applied field and vary with the frequency to some extent. It is necessary therefore, to determine the applied field and the frequency as well as the temperature in order to ensure accuracy' in describing the dielectric constant or dielectric loss. Because of the great influence of the applied field, the variations in dielectric constant by biasing field are utilized in dielectric amplifiers (Tanaka, 1954).

2.3.2. Electrostrictive Vibration:

In barium titanate ceramics, when the electric field is applied or once polarized under large field, can produce electrostrictive vibration as in the case of quartz. As to the modes of vibration, there are longitudinal length mode, radial mode, longitudinal thickness mode and shear

mode, though the last mentioned is rather difficult to realize because in this mode the direction of ramanent polarization and that of the filed should not be parallel. The coupling coefficient is largest in longitudinal thickness mode. Young's modulus E, Poisson's ratio σ and density ρ in barium titanate ceramics has the following values though they may be slightly different depending on how the materials are prepared: $E = 0.97 \cong 1.12 \times 10^{12} \text{ dyne/cm}^2$, $\sigma \cong 0.27$, $\rho = 5.5$

, and the power limit generally depends on the elastic limit of the ceramics. The acoustic power can be expressed as follows in equation (2.1).

$$P = \frac{1}{2} \frac{\rho_1}{\rho_0} \frac{V_1}{V_0} (\Delta p)^2 \dots\dots\dots (2.1)$$

Where ρ_1, V_1 are the density and the sound velocity of the liquid respectively, and ρ_0, V_0 are the density and the sound velocity of barium titanate ceramics. $(\Delta p)^2$ is the maximum stress in the interior of the vibrator and must be smaller than the mechanical strength of the vibrator (Tanaka, 1954) .

2.3.3. Electrostrictive and Piezoelectric Phenomena:

Barium titanate ceramics are aggregate of fine crystals and originally isotropic, but the applied field causes polarization parallel to the field and the piezoelectric phenomena. Once high voltage is applied, polarization remains even after the field is removed, and the ceramics continue to act as piezoelectric material for ever. But when the inverse field is applied, or heated beyond Curie point, the polarization decreases or disappears and the piezoelectric properties are lost. These facts are similar to those of the magnetization of ferromagnetic materials. The time required for magnetization is very short in magnetic materials, while that for barium titanate is comparatively long, the polarization being insufficient if the time is too short (Tanaka, 1954) .

2.3.4. Electronic and Magnetic Properties of Barium Titanate:

Perovskites with transition metal ions on the B site show an enormous variety of intriguing electronic or magnetic properties. This variety is not only related to their chemical flexibility, but it related to the complex character that transition metal ions play in certain coordinations with oxygen or halides . The magnetism and electronic correlations are usually related to unfilled 3d electron shells of the ions in the B site. Pronounced dielectric properties are connected with filled 3d electron shells. A coexistence of spontaneous ferroelectric and

ferromagnetic moments, is a rare phenomenon due to the small number of low-symmetry magnetic point groups that allow a spontaneous polarization. Nevertheless, in the presence of competing interactions canted moments or in composites large magneto-capacitive couplings have been reported (Johnsson and Lemmens, 2007) .

2.3.5. Structural Properties of Barium Titanate:

Barium titanate has structural properties which depend on temperature .There are two cases of structural properties of barium titanate. The first case at temperature $>120^{\circ}C$ the cubic structure of barium titanate will be formed with $a = 4.018\text{\AA}$ and the second case at temperature $< 120^{\circ}C$ the tetragonal structure of barium titanate will be formed with $a = 3.997\text{\AA}$, $c = 4.031\text{\AA}$ see figure (2.3a) and figure (2.3b). The tetragonal distortion leads to an off-centre displacement of Ti^{4+} and the dipoles are pointing along c axis, so the $BaTiO_3$ is ferroelectric material (Johnsson and Lemmens, 2007) .

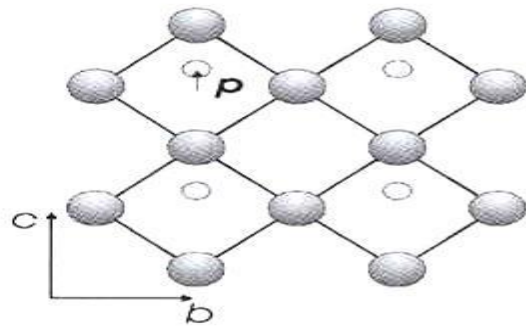
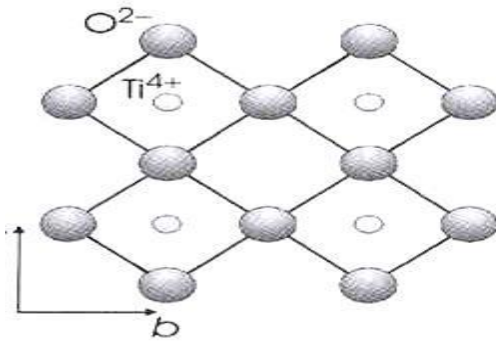


Figure (2.3a) cubic structure of $BaTiO_3$ [52] **Figure (2.3b)** tetragonal structure of $BaTiO_3$ (Johnsson and Lemmens, 2007) .

2.3.6. Optical properties of Barium Titanate:

Barium titanate has optical properties like transmittance, absorption, optical energy gap, reflective index. The optical properties of $BaTiO_3$ can be changed by doping material in $BaTiO_3$, where sometimes increase or decrease. The $BaTiO_3$ in its tetragonal phase, at room temperature, is a negative uniaxial crystal with relatively high refractive indices n_o, n_e , if compared with most other solids. The ordinary and extraordinary refractive indexes of un-doped $BaTiO_3$ at $20^{\circ}C$ are $n_o 2.412$ (Petruaru, 2003) .

CHAPTER THREE

Experimental Work

This chapter discussed the experimental work that includes fabrication and characterization techniques. Also, this chapter introduced the precursors that had been used to prepare the material. In addition, the samples were prepared in material science lab of physics department at Al-Neelain University.

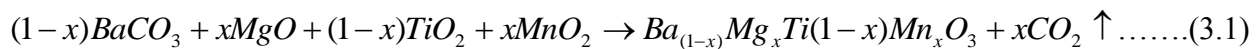
3.1. Solid-state reaction method:

During the last decades, the best method to prepare pure and doped barium titanate is solid state reaction by using mixed powders $BaCO_3$ and TiO_2 at high temperatures (1100-1400°C), due to its good properties such a low cost and the firing properties. It has many disadvantages like efficiency is too low and lose of some energy and the particles are not small enough, and (L. Wu et al., 2009).

3.2. Fabrication:

Five samples were prepared using solid state reaction method, and the $BaTiO_3$ is the main compound in this work that is doped with Mg in A site and Mn in B site. The prepared samples obeyed this formula $Ba_{(1-x)}Mg_xTi_{(1-x)}Mn_xO_3$ where $x = 0.01, 0.02, 0.03, 0.04, 0.05$. the following steps had followed to prepare the five samples below:

➤ This step includes weight the chemical equation as following :



➤ prepare the new material $Ba_{(1-x)}Mg_xTi_{(1-x)}Mn_xO_3$ using four precursors barium carbonate ($BaCO_3$) with purity (99.99%) , titanium dioxide (TiO_2) with purity (99.99%) , magnesium oxide (MgO) with purity (99.99%) , and manganese dioxide (MnO_2) with purity (99.99%). All of samples have been weighed using a sensitive electronic balance as shown in figure (3.1).

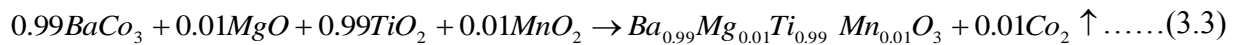
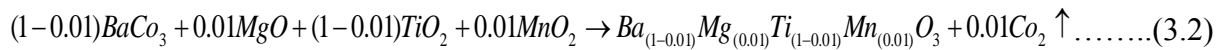


Figuer (3.1) KERN electronic balance
Capacity 120 g Readbility:0.1m

The caculation details of weights for five samples according to the concetation of the precursors, which mentioned at before by using the variation of them as shown as following:

$BaCo_3=197.34$ gm , $TiO_2= 79.87$ gm , $MgO= 40.31$ gm , and $MnO_2= 86.94$ gm .

For sample 1, $x = 1\% =0.01$, and the chemical equation will be :



$$BaCo_{3(0.99)} = (197.34)(0.99) = 195.3666 \text{ gm} , TiO_{2(0.99)} = (79.87)(0.99) = 79.0713 \text{ gm}$$

$$MgO_{(0.01)} = (40.31)(0.01) = 0.4031 \text{ gm} , MnO_{2(0.01)} = (86.94) (0.01) = 0.8694 \text{ gm}$$

The total of moceluar weights is =(195.3666 gm +79.0713 gm +0.4031 gm +0.8694 gm)
= 275.7104 gm .

$$\frac{BaCo_{3(0.99)}}{total} = \frac{195.3666}{275.7104} = 0.7086gm , \frac{TiO_{2(0.99)}}{total} = \frac{79.0713}{275.7104} = 0.2868gm$$

$$\frac{MgO_{(0.01)}}{total} = \frac{0.4031}{275.7104} = 0.0015gm , \frac{MnO_{2(0.01)}}{total} = \frac{0.8694}{275.7104} = 0.0032gm$$

Then , the total weight of samlpe 1 must be one gm (0.7086 gm+0.2868 gm+0.0015 gm+0.0032 gm=1 gm).

According to calculations above , the weights of five samples were calculated as shown in table (3.1) where x increased from 1% to 5%

Table (3.1) the weights of each sample is 1gm

NO	precursor	Sample 1	Sample 2	Sample 3	Sample 4	Sample 5
1	$BaCO_3$	0.7086 gm	0.7053 gm	0.7019 gm	0.6985 gm	0.6951 gm
2	TiO_2	0.2868 gm	0.2885 gm	0.2841 gm	0.2828 gm	0.2813 gm
3	MgO	0.0015 gm	0.0029 gm	0.0044 gm	0.0059 gm	0.0075 gm
4	MnO_2	0.0032 gm	0.0063 gm	0.0098 gm	0.0128 gm	0.0161 gm

To get five samples with two gm, the weights of five samples in the table (3.1) must be multiply by 2, which will be explained at the following :

For sample 1 :

$$BaCo_{3(0.99)} = (0.7086 \text{ gm}) (2) = 1.4172 \text{ gm} , TiO_{2(0.99)} = (0.2868) (2) = 0.5736 \text{ gm}$$

$$MgO_{(0.01)} = (0.0015 \text{ gm}) (2) = 0.003 \text{ gm} , MnO_{2(0.01)} = (0.0032) (2) = 0.0064 \text{ gm}$$

All of weights must be 2 grammes : $(1.41724 \text{ gm} + 0.5736 \text{ gm} + 0.003 \text{ gm} + 0.0064 \text{ gm}) = 2 \text{ gm} .$

Based on caculations which mention before , the weights of five samples were calculated as shown in table (3.2) where x increased from 1% to 5%

Table (3.2) the weight of each sample is 2gm

NO	precursor	Sample 1	Sample 2	Sample 3	Sample 4	Sample 5
1	$BaCO_3$	1.4172 gm	1.4106 gm	1.4038 gm	1.397 gm	1.3902 gm
2	TiO_2	0.5736 gm	0.5710 gm	0.5682 gm	0.5656 gm	0.5626 gm
3	MgO	0.003 gm	0.0058 gm	0.0088 gm	0.0118 gm	0.015 gm
4	MnO_2	0.0064 gm	0.0126 gm	0.0192 gm	0.0256 gm	0.0322 gm

- The Powders were mixed in a great mortar for 2hours with acetone to get a homogeneous precursors as shown in figure (3.2) .



Figure (3.2) a great mortar equipment

- Five samples were heated in the laboratory oven at $200^{\circ}C$ for 4 hours because it is necessary to get a homogeneous compounds as shown in figure (3.3) .



Figuer(3.3): laboratory oven (lab-tech), volt 230, watts 500
Serial No: 14125, size: 14x14, Manufacturing in India

- Before heating, all five samples were put in five crucibles as shown in figure (3.4), and they pressed as disc samples .
- All samples were calcinated at $1200^{\circ}C$ for 5 hours until the five samples were formed using an oven (CARBOLITE) as shown in figure (3.5).



Figuer(3.4): Five Crucibles



Figuer(3.5): CARBOLITE –CWF 1200° C

Serial No: 20-302426, Manufacturing in England

- Each sample became very strong crystals, and they grinded as powder samples using a great mortar equipment.

3.3. Characterization Techniques:

The optical and structural properties of $Ba_{(1-x)}Mg_xTi_{(1-x)}Mn_xO_3$ where $x = 0.01, 0.02, 0.03, 0.04, 0.05$ were studied using the XRD spectroscopy, FTIR spectroscopy, and Uv-visible spectroscopy as shown following :

3.3.1. Prepration samples for XRD spectroscopy :

All five samples were pressed, and they put incide the holder of XRD device to record the XRD diffractions for five samples as shown at figure (3.6). On other hand , these sreults were done at the lab of Ministry of Oil and Minerals in Republic of Sudan.



Figure (3.6) Phelps XRD, Serial number: 943003040601, Manufactured in Holland

3.3.2. Principle of X-ray Diffraction Spectroscopy:

X-ray photons are a form of electromagnetic radiation produced following the ejection of an inner orbital electron subsequent transition of atomic orbital electrons from states of high to low energy. When a monochromatic beam of X-ray photons falls onto a given specimen three basic phenomena may result, namely absorption, scatter or fluorescence. The coherently scattered photons may undergo subsequent interference leading in turn to the generation of diffraction maxima. These three basic phenomena form the bases of three important X-ray methods: the absorption technique, which is the basis of radiographic analysis; the scattering effect, which is the basis of X-ray diffraction; and the fluorescence effect, which is the basis of XRD spectrometry (Jenkins, 2000). The X-ray diffraction cnoformed by Bragss law at below :

$$n\lambda = 2d \sin \theta \dots\dots\dots (3.4)$$

Where n is an integer , λ is the wavelenght , d is the diatance between two levels , and θ is scattering angle (Jenkins, 2000)

3.3.3. Prepration Samples for FTIR Spectroscopy:

The KBr pressed disc technique is the most widely used for preparing a solid sample for routine scanning of the spectra .Each sample mixed with dry potassuim bromide powder . Bn applying sufficient presure , the mixture was pressed into a transparent disc . the usual KBr was 1:100 as shown in figure (3.7) .



Figure (3.7)... Satellite FTIR ... Serial N0 20010102
Voltage. +5/+15/-15 VDC... Manufactured in U.S.A

3.3.4. Principle of FTIR Spectroscopy:

FTIR spectroscopy is a technique which describes the interaction between the radiation and a sample that can be solid, liquid or gaseous. This technique measures the frequencies and the intensities of these absorptions. The spectrum can be represented by two-dimensional where the x,y axes denotes to the wave number and the transmittance respectively. The peaks of frequencies are helpful for the identification of the sample's chemical bonds and functional groups which responsible for the absorption of radiation at different frequencies.. The infrared region of the electromagnetic spectrum extends from the visible to the microwave as shown in figure (3.8) (Petraru, 2003).

The Electromagnetic Spectrum

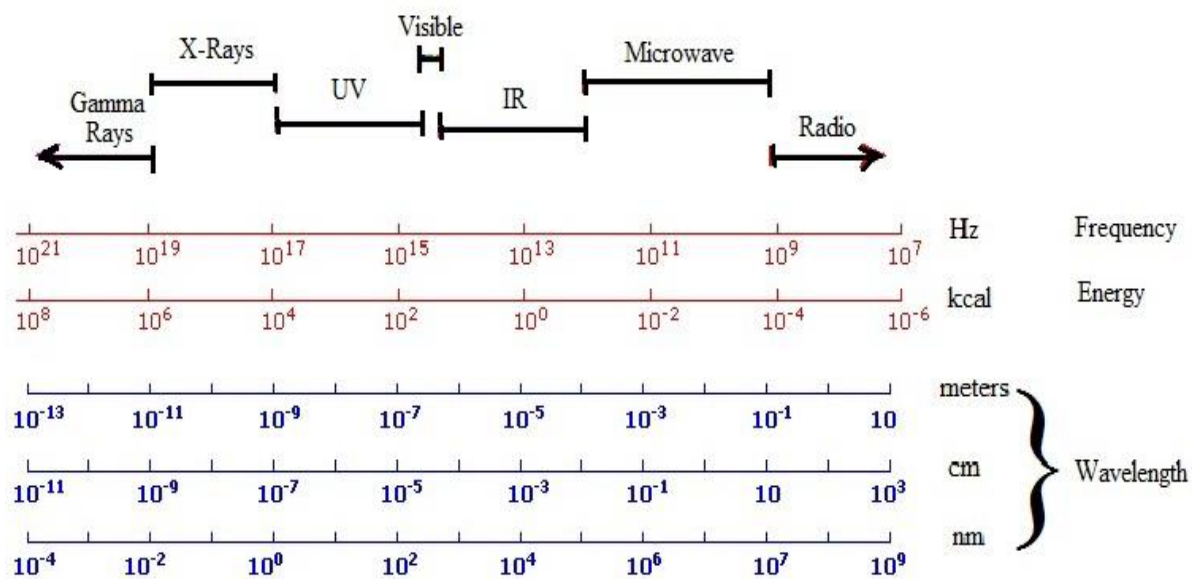


Figure (3.8) schematic representation of the electromagnetic spectrum (Petraru, 2003)

3.3.5. preparation samples for Uv-visible spectroscopy :

This technique was used with a weight of 0.01 gm and was dissolved in 10 ml of distilled water. The source was calibrated by distilled water. The absorption spectra of the five dissolved samples was recorded in the Uv-Visible device as shown in figure (3.9).



Figure (3.9) UV mini- 1240 CE... Serial No A10934081718 Sm
220- 240 V- 50 / 60HZ – 160 VA Manufactured in Germany

3.3.6. Principle of UV-visible Spectroscopy :

The UV-visible spectroscopy is the radiation comprise only a small portion of wavelengths from about $10^{-6} m - 10^{-7} m$, where the spectrum of electromagnetic radiation as a whole spans the range of wavelengths (λ) from $10^{10} m$ (infrasound) down to $10^{14} m$ (cosmic radiation). For all types of electromagnetic radiation, the associated energy (E) is calculated using Planck's constant:

$$E = h \times \nu \dots\dots\dots(3.5)$$

Where (E) is energy , h Planck's constant ($6.626 \times 10^{-34} J.S^{-1}$), and ν is frequency S^{-1} . The frequency of the radiation is calculated according to the following equation:

$$\nu = \frac{C}{\lambda} \dots\dots\dots(3.6)$$

Where C is velocity of light ($3 \times 10^8 \frac{m}{s}$), and λ Wavelength in m . In UV/VIS spectroscopy, wavelengths are usually expressed in nanometers ($nm = 10^{-9} m$) (Owen, 1996).

3.3.7. The Beer-Lambert Law :

The basic principles that can be used to quantify light absorption in solutions were recognized early. In the 18th century, Lambert and Bouguer found that, at a constant concentration, differential light absorption was proportional to path length . The combination of that law with Beer's law, which states that light absorption in a colored solution is proportional to the concentration of the substance dissolved in a colorless solvent, leads to what is known as the Beer-Lambert law (Owen, 1996).

$$T = \frac{I}{I_0} = e^{-\epsilon_{\lambda}cd} \dots\dots\dots(3.7)$$

Where T is transmittance ,I is intensity of transmitted light, I_0 is Intensity of incident light, ϵ_{λ} is Extinction coefficient at a given wavelength , C is concentration , and d is the Path length .

The Beer-Lambert law is best known in its logarithmic form:

$$E_{\lambda} = -\log T = \log \frac{I_0}{I} = \epsilon_{\lambda} \times C \times d \dots\dots\dots(3.8)$$

Where E_{λ} is Extinction at a given wavelength (Owen, 1996).

CHAPTER FOUR

Results and Discussion

This chapter includes the results and discussion of the prepared sample $\text{Ba}_{(1-x)}\text{Mg}_x\text{Ti}_{(1-x)}\text{Mn}_x\text{O}_3$ where $(x) = 0.01, 0.02, 0.03, 0.04, 0.05$.

4.1. XRD Analysis:

The five samples of $\text{Ba}_{(1-x)}\text{Mg}_x\text{Ti}_{(1-x)}\text{Mn}_x\text{O}_3$ where $(x) = 0.01, 0.02, 0.03, 0.04, 0.05$ have been analyzed using XRD spectroscopy as shown in figures from (4.1) at below:

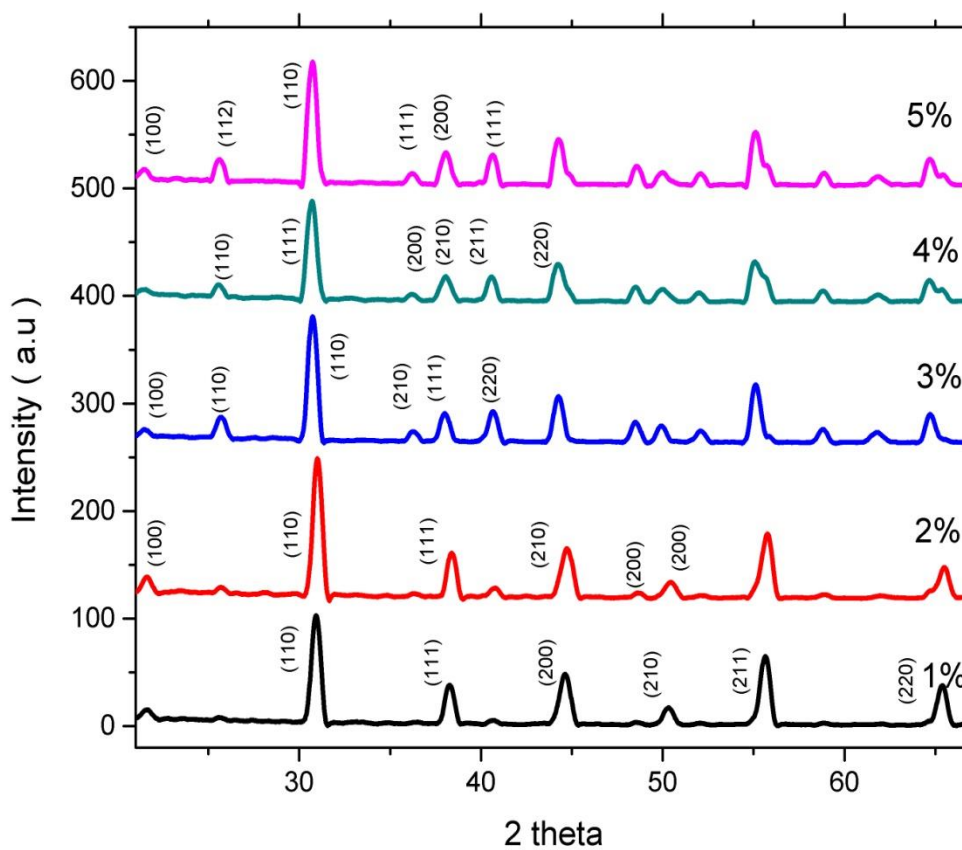


Figure (4.1) XRD combined for all five samples

For sample 1 when x= 1%

Table (4.1) the XRD results of $\text{Ba}_{0.99}\text{Mg}_{0.01}\text{Ti}_{0.99}\text{Mn}_{0.01}\text{O}_3$ single perovskite oxide

2 theta (θ°)	D(A°)	H	K	L	a (A°)	b (A°)	c (A°)	Average of lattice constants (a,b,c) (A°)	α, β, γ (θ°)
30.971	2.8850	1	1	0	4.0800	4.0800	4.0800	4.0512	90°
38.291	2.3487	1	1	1	4.0680	4.0680	4.0680	4.0512	90°
44.867	2.0185	2	0	0	4.0370	4.0370	4.0370	4.0512	90°
50.384	1.8096	2	1	0	4.0465	4.0465	4.0465	4.0512	90°
55.649	1.6502	2	1	1	4.0423	4.0423	4.0423	4.0512	90°
65.388	1.4260	2	2	0	4.0334	4.0334	4.0334	4.0512	90°

For sample 2 when x= 2%

Table (4.2) the XRD results of $\text{Ba}_{0.98}\text{Mg}_{0.02}\text{Ti}_{0.98}\text{Mn}_{0.02}\text{O}_3$ single perovskite oxide

2 theta (θ°)	D(A°)	h	k	l	a(A°)	b(A°)	c(A°)	Average of lattice constants (a,b,c) (A°)	α, β, γ (θ°)
21.732	4.0860	1	0	0	4.0800	4.0800	4.0800	4.2086	90°
31.068	2.8762	1	1	0	4.0676	4.0676	4.0676	4.2086	90°
38.449	2.3393	1	1	1	4.0518	4.0518	4.0518	4.2086	90°
40.885	2.2054	2	1	0	4.9315	4.9315	4.9315	4.2086	90°
44.335	2.0415	2	0	0	4.0829	4.0829	4.0829	4.2086	90°
44.931	1.0158	2	0	0	4.0315	4.0315	4.0315	4.2086	90°

For sample 3 when x= 3%

Table (4.3) the XRD results of $Ba_{0.97}Mg_{0.03}Ti_{0.97}Mn_{0.02}O_3$ single perovskite oxide

2 theta (θ°)	d(A°)	H	K	L	a(A°)	b(A°)	c(A°)	Average of lattice constants (a,b,c) (A°)	α, β, γ (θ°)
21.488	4.1320	1	0	0	4.1320	4.1320	4.1320	5.0087	90°
25.868	3.4414	1	1	0	5.9607	5.9607	5.9607	5.0087	90°
30.807	2.9000	1	1	0	4.1012	4.101 2	4.1012	5.0087	90°
36.334	2.4705	2	1	0	5.5243	5.5243	5.5243	5.0087	90°
38.048	2.3631	1	1	1	4.0930	4.0930	4.0930	5.0087	90°
40.864	2.2065	2	2	0	6.2410	6.2410	6.2410	5.0087	90°

For sample 4 when x= 4%

Table (4.4) the XRD results of $Ba_{0.96}Mg_{0.04}Ti_{0.96}Mn_{0.04}O_3$ single perovskite oxide

2 theta (θ°)	d(A°)	H	K	L	a(A°)	b(A°)	c(A°)	Average of lattice constants (a,b,c) (A°)	α, β, γ (θ°)
25.607	3.4759	1	1	0	4.9157	4.9157	4.9157	5.1955	90°
30.669	2.9127	1	1	1	5.0449	5.0449	5.0449	5.1955	90°
37.972	2.3676	2	0	0	4.7353	4.7353	4.7353	5.1955	90°
38.299	2.3482	2	1	0	5.2506	5.2506	5.2506	5.1955	90°
40.649	2.2177	2	1	1	5.4322	5.4322	5.4322	5.1955	90°
44.179	2.0485	2	2	0	5.7941	5.7941	5.7941	5.1955	90°

For sample when $x=5\%$

Table (4.5) the XRD results of $Ba_{0.95}Mg_{0.05}Ti_{0.95}Mn_{0.05}O_3$ single perovskite oxide

2 theta (θ°)	d(A°)	H	K	L	a(A°)	b(A°)	c (A°)	Average of lattice constants (a,b,c)(A°)	α, β, γ (θ°)
21.444	4.1404	1	0	0	4.1404	4.1404	4.1404	5.0184	90°
25.667	3.4679	1	1	2	8.4945	8.4945	8.4945	5.0184	90°
30.651	2.9144	1	1	0	4.1216	4.1216	4.1216	5.0184	90°
36.092	2.4865	1	1	1	4.3068	4.3068	4.3068	5.0184	90°
36.327	2.4710	2	0	0	4.9420	4.9420	4.9420	5.0184	90°
37.931	2.3701	1	1	1	4.1051	4.1051	4.1051	5.0184	90°

The results of XRD in figure (4.1), and the tables from (4.1) to (4.5) confirm that the synthesized samples have a cubic phase, which agree with results as proved by (Zhu et al., 2011), (Langhammer et al., 2000b), (Badapanda et al., 2016), (Wang et al., 2006), (Emre et al., 2014), and (Cui et al., 2006). On the other hand, the strongest diffraction of sample 1 at 30.971° , sample 2 at 31.068° , sample 3 at 30.807° , sample 4 at 30.669° , and sample 5 at 30.651° , which are in a good agreement with results as documented by all researches in chapter 2. In addition, the average of lattice constants and grain sizes increased with dopant from sample 1 to sample 4 ($4.0512A^\circ$, $4.2086A^\circ$, $5.087A^\circ$, and $5.1955A^\circ$) and (29.3nm, 32.4nm, 36.15 nm, and 37.98 nm) respectively. On the other hand, the lattice constants and grain size decreased with Mg and Mn contents in sample 5 ($5.0184A^\circ$), (37.5 nm) respectively which agree with results as documented by (Hao et al., 2011), and these results of the average lattice constants and grain size is related to the change in the position of atoms after doping in barium titanate by Mg and Mn elements, and the occupations of atoms during the calcinations process. In the figure (4.1), there are some abroad peaks at sample 4 and 5, and these results may be related to the radius of atoms and the density of diffraction.

Table (4.6) comparing between the average of lattice constants and grain sizes of the five samples:

NO	Sample	The average of lattice constants	The average of grain size
1	$\text{Ba}_{0.99}\text{Mg}_{0.01}\text{Ti}_{0.99}\text{Mn}_{0.01}\text{O}_3$	4.0512 \AA°	29.3 nm
2	$\text{Ba}_{0.98}\text{Mg}_{0.02}\text{Ti}_{0.98}\text{Mn}_{0.02}\text{O}_3$	4.2086 \AA°	32.4 nm
3	$\text{Ba}_{0.97}\text{Mg}_{0.03}\text{Ti}_{0.97}\text{Mn}_{0.02}\text{O}_3$	5.0087 \AA°	36.15 nm
4	$\text{Ba}_{0.96}\text{Mg}_{0.04}\text{Ti}_{0.96}\text{Mn}_{0.04}\text{O}_3$	5.1955 \AA°	37.98 nm
5	$\text{Ba}_{0.95}\text{Mg}_{0.05}\text{Ti}_{0.95}\text{Mn}_{0.05}\text{O}_3$	5.0184 \AA°	37.5 nm

From figure (4.1), the obtained results displayed that the intensity increased for sample 1, samples 2, sample 3, and sample 5 with increasing contents of dopant in the barium titanate ceramics, but it decreased in sample 4, and this result attributed to ionic radius of atoms and the density of diffractions.

4.2. FTIR Analysis:

Five samples of $\text{Ba}_{(1-x)}\text{Mg}_x\text{Ti}_{(1-x)}\text{Mn}_x\text{O}_3$ where $(x) = 0.01, 0.02, 0.03, 0.04, 0.05$. were analyzed using FTIR spectroscopy as shown from fig (4.2) below:

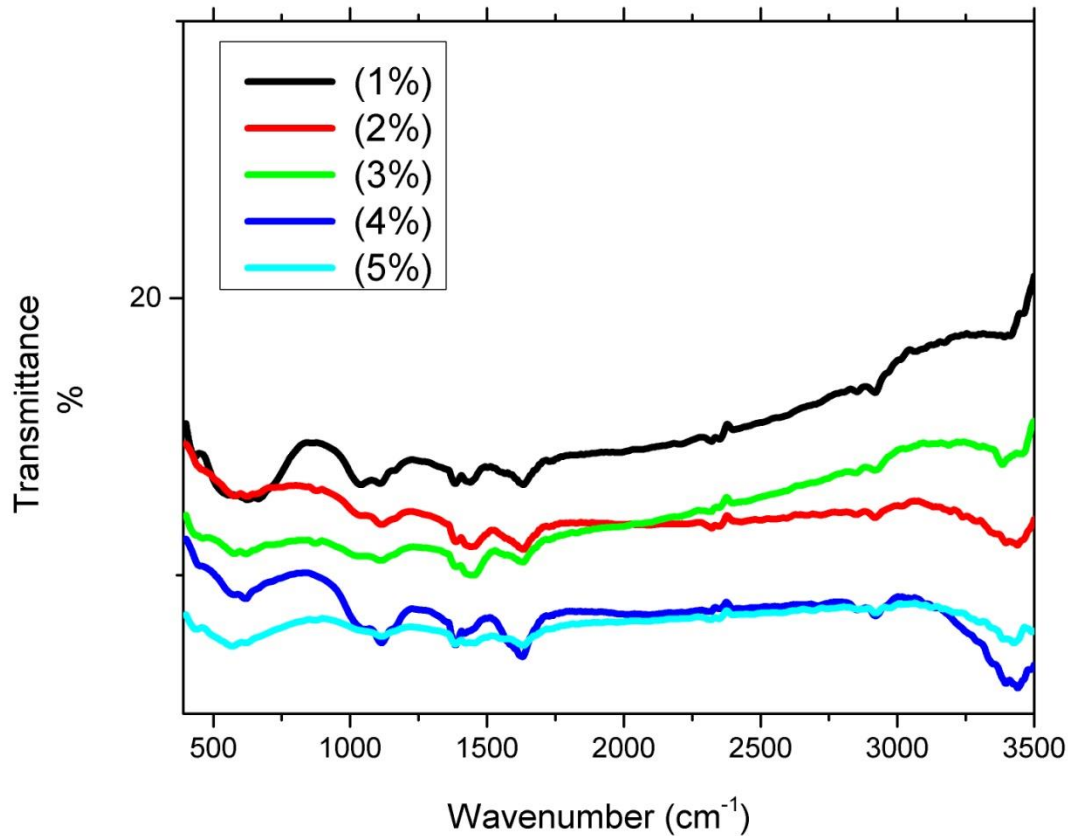


Figure (4.2) FTIR spectrum of combined for all five samples

By using the zoom, the results for sample 1 in figure (4.2) show that the peak around 431cm^{-1} is due to Ti-O bending (García-Hernández et al., 2013). Also, the peak at 510cm^{-1} is caused by (Mn-O-Mn) Stretching (Korman.,et al.,2011), Mn-O stretching (García-Hernández et al., 2013), and Ti-O strong stretching (Cui et al., 2006). However, the peaks at 625cm^{-1} and 673cm^{-1} indicated to the presence of Ti-O-Ti strong stretching bond (Cui et al., 2006), and Mn-O stretching (García-Hernández et al., 2013). On the other hand, the possible to existence of alcohols, carboxylic acids, esters, anhydrides, ethers compounds for C-O strong stretching were appeared at peaks 1013cm^{-1} , 1038cm^{-1} , 1124cm^{-1} , 1160cm^{-1} (Pavia et al., 2008). The group of

– CH_3 can be appeared at the peaks 1434 cm^{-1} and 1378 cm^{-1} is due to C-H bend medium, and the peak at 1634 cm^{-1} is due to C=C alkene medium band (Pavia et al.,2008) . The existence of alcohols and phenols groups for O-H medium stretching observed at the peaks 2320 cm^{-1} , 2350 cm^{-1} , 2848 cm^{-1} , 2915 cm^{-1} , 3012 cm^{-1} , 3060 cm^{-1} , 3178 cm^{-1} , 3412 cm^{-1} , and 3461 cm^{-1} (Pavia et al., 2008) .

The spectrum of sample 2 in figure (4.2), the results display that the peaks 641 cm^{-1} and 450 cm^{-1} is due to (Ti-O-Ti) bending, and it is caused by Mn-O stretching (Ashiri and Helisaie., 2011). Also, the peak at 490 cm^{-1} is caused by (Ti-O) strong Stretching (Cui et al., 2006). On the other hand, 732 cm^{-1} indicated to presence of N-H strong stretching bond (Pavia et al., 2008), and the possible to presence of alcohols, carboxylic acids esters ethers, anhydrides compounds for C-O strong stretching were appeared at peaks 1021 cm^{-1} , 1075 cm^{-1} , 1279 cm^{-1} (Pavia et al., 2008). However, the existance of alcohols and phenols gropus for O-H medium stretching band observed at the peaks 2544 cm^{-1} , 2609 cm^{-1} , 2710 cm^{-1} , 2839 cm^{-1} , 2941 cm^{-1} , 3102 cm^{-1} , and 3151 cm^{-1} , 3306 cm^{-1} , 3365 cm^{-1} , and 3424 cm^{-1} (Pavia et al., 2008) .

The result of spectra for sample 3 in figure (4.2) indicate that the peak at 490 cm^{-1} is caused by (Ti-O) strong Stretching (Cui et al., 2006), and the peak at 737 cm^{-1} indicated to presence of N-H strong stretching bond (Pavia et al., 2008) . Also, the possible to presence of alcohols, carboxylic, acids, esters, ethers, and anhydrides compounds for C-O strong stretching were appeared at peaks 1016 cm^{-1} , 1075 cm^{-1} , 1274 cm^{-1} (Pavia et al., 2008). However, the existance of alcohols and phenols groups for O-H medium stretching band observed at the peaks 2540 cm^{-1} , 2620 cm^{-1} , 2893 cm^{-1} , 3091 cm^{-1} , 3311 cm^{-1} , 3371 cm^{-1} , 3424 cm^{-1} , 3445 cm^{-1} (Pavia et al., 2008) .

In figure (4.2), the result of sample 4 show that the peak at 563 cm^{-1} is caused by (Mg-O) Stretching (Korman et al.,2011) , and the peak around 668 cm^{-1} is due to (Ti-O-Ti) bending the (Ashiri and Helisaie,2011) . Also, the peaks at 742 cm^{-1} , 792 cm^{-1} indicated to presence of N-H strong stretching bond (Pavia et al., 2008), and the possible to presence of alcohols, carboxylic acids esters ethers, and anhydrides compounds for C-O strong stretching were appeared at peaks 1019 cm^{-1} , 1272 cm^{-1} (Pavia et al., 2008) .On the other hand, the peaks at 1985 cm^{-1} and 2400 cm^{-1} is due to medium O-H vibration for carboxylic acids (Pavia et al., 2008). However, existance of alcohols and phenols gr within gropus for O-H

medium stretching band observed at the peaks 2544 cm^{-1} , 2613 cm^{-1} , 2796 cm^{-1} , 3058 cm^{-1} , 3108 cm^{-1} , 3162 cm^{-1} , 3212 cm^{-1} , 3257 cm^{-1} , 3390 cm^{-1} , 3439 cm^{-1} (Pavia et al., 2008).

The spectra of sample 5 in the figure (4.2), the result confirm that the peak at 563 cm^{-1} is caused by (Mg-O) Stretching (Korman et al., 2011), and the peak at 668 cm^{-1} is due to (Ti-O-Ti) bending (Ashiri and Helisaie, 2011). In around 742 cm^{-1} , 792 cm^{-1} indicated to presence of N-H strong stretching bond (Pavia et al., 2008). Also, the possible to presence of alcohols, carboxylic acids esters ethers, and anhydrides compounds for C-O strong stretching were appeared at the peaks 1021 cm^{-1} , 1064 cm^{-1} , 1139 cm^{-1} , 1198 cm^{-1} , 1278 cm^{-1} . On the other hand, the peak at 1327 cm^{-1} is caused to amines of C-N medium and strong band (Pavia et al., 2008), and the peak at 1740 cm^{-1} is due to C=O strong band for aldehydes (Pavia et al., 2008). However, the to existence of carboxylic acids group for O-H medium stretching band observed at the peaks 2532 cm^{-1} , 2555 cm^{-1} , 2620 cm^{-1} , 2668 cm^{-1} , 2710 cm^{-1} , 2790 cm^{-1} , 2828 cm^{-1} , 2860 cm^{-1} , 2909 cm^{-1} , 2984 cm^{-1} , 3008 cm^{-1} , 3097 cm^{-1} , 3140 cm^{-1} , 3214 cm^{-1} , 3257 cm^{-1} , 3310 cm^{-1} , 3355 cm^{-1} , 3371 cm^{-1} , 3408 cm^{-1} , and 3461 cm^{-1} (Pavia et al., 2008).

By using the zoom in figure (4.2), The results of FTIR spectroscopy which mention before confirmed that the existence of the band Mn-O-Mn stretching and bending was appeared only in sample 1 which was documented by (Korman et al., 2011). Also, the Ti-O bending band was found in sample 1 and sample 2, which were in a good agreement with (Langhammer et al., 2000a), (Mohamed and Dughaiash, 2012), (García-Hernández et al., 2013), and (Cui et al., 2006). In addition, the Ti-O stretching band was investigated in sample 1, sample 2, and sample 3, but it was not appeared in samples 4 and 5 which were in a good agreement with (Zhu et al., 2011), (Kaur et al., 2016), (Sengodan et al., 2012), and (Ashiri and Helisaie., 2011). Furthermore, the Ti-O-Ti strong stretching band was showed just in sample 1 which was documented by (Langhammer et al., 2000a). Moreover, the Ti-O-Ti bending band was appeared only in sample 2, sample 4, and sample 5 which were confirmed by (Kaur et al., 2016), and (Ashiri and Helisaie., 2011). On other hand, the Mn-O stretching band was just appeared in sample 1 and sample 2 which was documented by (Korman et al., 2011).

These results proved the presence of the N-H stretching band was only appeared in samples 2, 3, 4, and 5. Also, the C-O strong stretching band was displayed in samples 1, 2, 3, 4, and 5 which was documented by (Zhu et al., 2011), (Langhammer et al., 2000a), (García-Hernández et al., 2013), (Emre et al., 2014), and (Ashiri and Helisaie., 2011). In

addition, the C-H bending band with group $-CH_3$ was just appeared at sample 1, and the C-N medium and strong band was appeared at sample 5. Furthermore, the C=O medium band was only displayed at sample1 which was documented by (Bisen et al., 2016) .However , the O-H stretching band was showed at all five samples which were proved by (Hao et al., 2011) , (Bisen et al., 2016) , (Langhammer et al., 2000a) , (Mohamed and Dughhaish, 2012) , (Sengodan et al., 2012) , and (Emre et al.,2014) .

In the figure (4.7), all five samples have many identical frequencies at the peaks 625 cm^{-1} , 1038 cm^{-1} , 1112 cm^{-1} , 2915 cm^{-1} . On the other hand, the prepared samples have small shifts at some peaks as shown in the table (4.1), and these shifts are associated with ionic raduis of doped elements. The frequencies values displayed that the ratio of transmittance decreased with dopant of Mg and Mn , and this decreasing of the transmittance may be related to increasing of density for samples which caused to increasing of grain size (Al-Jumaili., et al 2011).

Table (4.7) the identical and shifted FTIR absorption bonds for all five samples:

NO Sample	ν_1 (cm^{-1})	ν_2 (cm^{-1})	ν_3 (cm^{-1})	ν_4 (cm^{-1})	ν_5 (cm^{-1})	ν_6 (cm^{-1})	ν_7 (cm^{-1})	ν_8 (cm^{-1})	ν_9 (cm^{-1})	ν_{10} (cm^{-1})	ν_{12} (cm^{-1})	ν_{13} (cm^{-1})	ν_{14} (cm^{-1})
$Ba_{0.99}Mg_{0.01}Ti_{0.99}Mn_{0.01}O_3$	431	571	625	1038	1112	1384	1439	1634	2314	2350	2855	2915	3400
$Ba_{0.98}Mg_{0.02}Ti_{0.98}Mn_{0.02}O_3$	436	571	625	1038	1112	1384	1439	1627	2314	2345	2855	2915	3377
$Ba_{0.97}Mg_{0.03}Ti_{0.97}Mn_{0.03}O_3$	437	577	625	1038	1112	1390	1445	1627	2320	2345	2848	2915	3400
$Ba_{0.96}Mg_{0.04}Ti_{0.96}Mn_{0.04}O_3$	437	577	625	1038	1112	1384	1445	1627	2314	2350	2855	2915	3395
$Ba_{0.95}Mg_{0.05}Ti_{0.99}Mn_{0.05}O_3$	437	571	625	1038	1112	1384	1445	1627	2314	2345	3855	2915	3395

4.3. UV-Visible Analysis:

Five samples of $\text{Ba}_{(1-x)}\text{Mg}_x\text{Ti}_{(1-x)}\text{Mn}_x\text{O}_3$ where $(x) = 0.01, 0.02, 0.03, 0.04, 0.05$. were analyzed by UV-visible spectroscopy, as shown in figure (4.3) below:

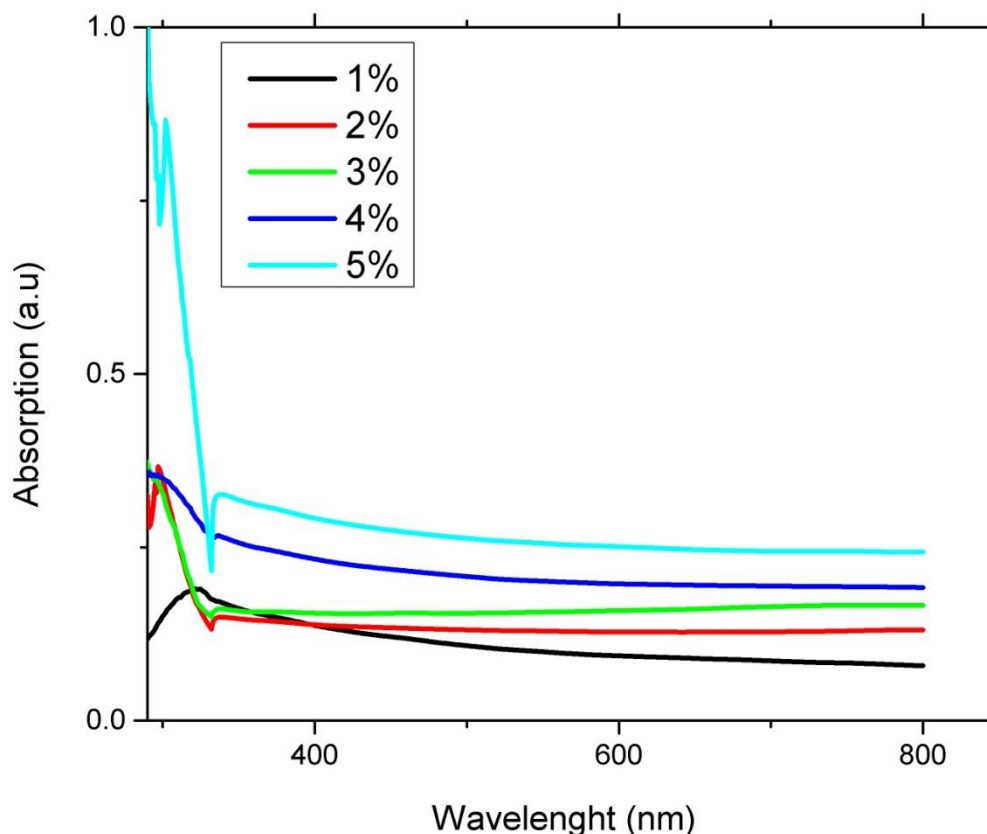


Figure (4.3) UV- visible absorption combined for all five samples

From the spectrum in figure (4.3), the absorption of sample 1 when $x = 0.01$ were found at (0.189 a.u) with maximum wavelength at 322.6 nm. Also, the absorption of sample 2 where $x = 0.02$ were found at (0.340 a.u) with the maximum wavelength at 297.4 nm. Furthermore, the absorption of sample 3 where $x = 0.03$ were found at (0.346 a.u) with the maximum wavelength at 293.9 nm. Moreover, the absorption of sample 4 single preovskite oxide where $x = 0.04$ were found at (0.355 a.u) with maximum wavelength at 292.4 nm. Finally, the absorption of sample 5 single preovskite oxide where $x = 0.05$ were found at (0.910) with the maximum wavelength at 291.9 nm.

In the figure (4.3), all five samples have one identical peak that can be shown above, and the results show that the absorption increased with increasing of doping

for Mg, Mn at barium titanate .This increasing related to increasing in grain size of the prepared samples, and they became more transparent with increasing of dopant (Al-Jumaili., et al 2011).

4.4. Calculation of Optical Band Gap Energy:

The optical band gap energy (E_g) for all five samples of single preovskite oxide $Ba_{(1-x)}Mg_xTi_{(1-x)}Mn_xO_3$ where $(x) = 0.01, 0.02, 0.03, 0.04, 0.05$ has been calculated by the relation:

$$(\alpha h\nu)^2 = C(h\nu - E_g) \dots\dots\dots (4.1)$$

Where C is constant , ($h\nu$) is photon energy, (α) is absorption coefficient (Simon M. Sze, Kwok K. Ng,2006). The obtained band gap energy can be found for all five samples using the tangent as displayed in figure (4.4) below:

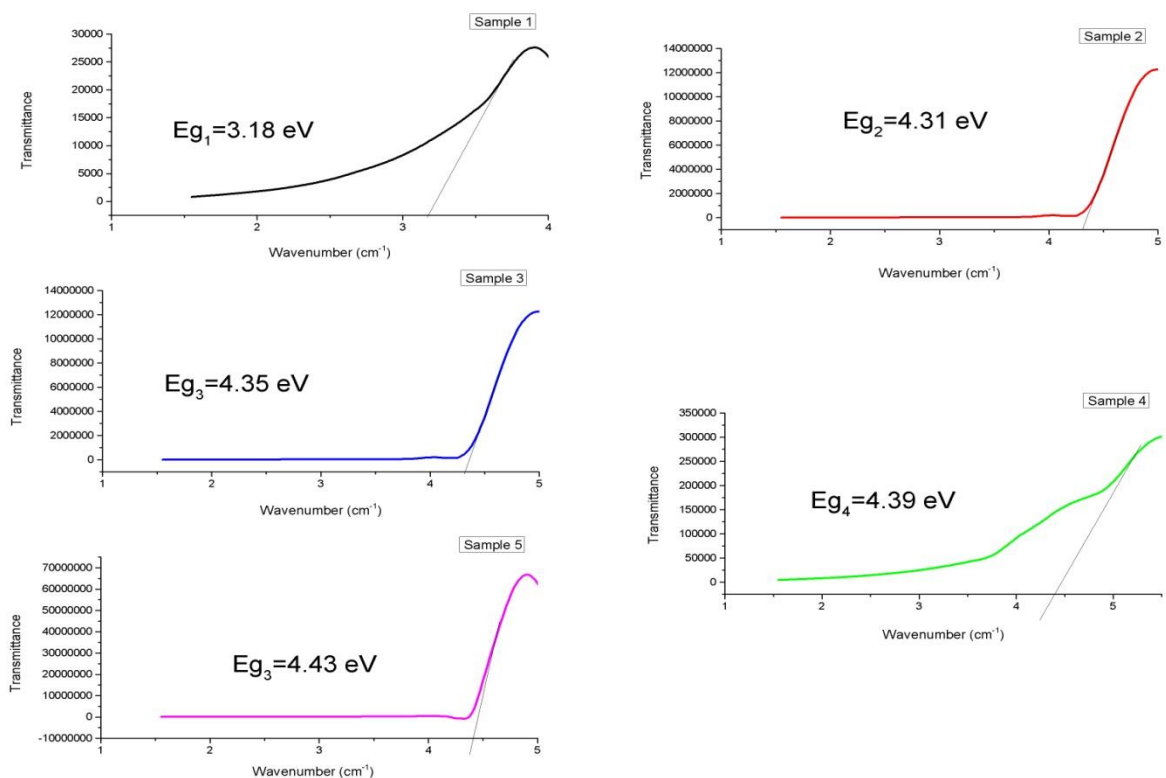


Figure (4.4) Optical band gap energy combined for all five samples

By extrapolation the straight thin portion of the curve to intercept the energy axis .the value of optical band gap energy for sample 1 was 3.18 eV, for sample 2 was 4.31 eV, for sample 3 was 4.35 eV, for sample 4 was 4.39 eV, and sample 5 was 4.43

eV as displayed in figure (4.4) Also, the results at above confirmed that the band gap energy increased with increasing of Mg and Mn contents at $BaTiO_3$, which disagree with results as documented by (Badapanda et al ., 2016) and (Mohamed and Dughaish, 2012) .The increasing of optical energy band gap may be related to increasing of in grain boundaries and their density duo to heating effect for the crystals of samples (Al-Jumaili., et al 2011) , and these results disagree with results as documented by (Badapanda et al ., 2016) and (Mohamed and Dughaish, 2012).

4.5. Calculation of Refractive Index:

The refractive index (n) was calculated using the relation $n = 3.3668(Eg)^{-0.3224}$ (Imam, 2017), and the refractive indexes decreased with increasing of Mg, Mn concentration (2.31, 2.10, 2.09, 2.089, and, 2.083) respectively. These results was agree with research (Eswaramoorthi et al., 2015) , and these results disagree with results as documented by (Badapanda et al ., 2016) and (Mohamed and Dughaish, 2012).

Sample 1:

$$n_1 = 3.3668(3.18)^{-0.3224} = 2.31 \dots\dots\dots (4.1)$$

By the same steps above, the values for refractive index of $Ba_{(1-x)}Mg_xTi_{(1-y)}Mn_yO_3$, where x,y =0.01, 0.2, 0.03, 0.4, and 0.05 as shown in table (4.2) .

Table (4.8) the values of refractive index of five samples

No	Sample	Refractive index
1	$Ba_{0.99}Mg_{0.01}Ti_{0.99}Mn_{0.01}O_3$	2.31
2	$Ba_{0.98}Mg_{0.02}Ti_{0.98}Mn_{0.02}O_3$	2.10
3	$Ba_{0.97}Mg_{0.03}Ti_{0.97}Mn_{0.03}O_3$	2.09
4	$Ba_{0.96}Mg_{0.04}Ti_{0.96}Mn_{0.04}O_3$	2.089
5	$Ba_{0.95}Mg_{0.05}Ti_{0.99}Mn_{0.05}O_3$	2.083

The refractive index of pure barium titanate is 2.360 (Petraru, 2003), and the decreasing of reflective index of dopant in all samples above may be related to the samples became more transparent with increasing of Mg and Mn contents (Al-Jumaili., et al 2011) .

Table (4.9) comparing between Uv-Visible results

No	Sample	Band gap energy (Eg)	Maximum wavelength (nm)	Absorption (a.u)	Refractive index (n)
1	$Ba_{0.99}Mg_{0.01}Ti_{0.99}Mn_{0.01}O_3$	3.18	322.6 nm	0.189 (a.u)	2.31
2	$Ba_{0.98}Mg_{0.02}Ti_{0.98}Mn_{0.02}O_3$	4.31	297.4 nm	0.340 (a.u)	2.10
3	$Ba_{0.97}Mg_{0.03}Ti_{0.97}Mn_{0.03}O_3$	4.35	293.9 nm	0.346 (a.u)	2.09
4	$Ba_{0.96}Mg_{0.04}Ti_{0.96}Mn_{0.04}O_3$	4.39	292.4 nm	0.355 (a.u)	2.089
5	$Ba_{0.95}Mg_{0.05}Ti_{0.99}Mn_{0.05}O_3$	4.43	291.9 nm	0.910 (a.u)	2.083

CHAPTER FIVE

Conclusion and Recommendation

5.1. Conclusion:

Five samples of single perovskite oxides of $Ba_{(1-x)}Mg_xTi_{(1-x)}Mn_xO_3$, where $x=0.01, 0.2, 0.03, 0.4$, and $0, 05$ have been successfully prepared using solid state reaction method, and their structural and optical properties were studied by XRD, FTIR, and UV-visible techniques.

The XRD results proved that the prepared samples had a cubic phase, and the strongest peaks of the diffraction which mentioned before confirmed that the structure of single perovskite has been formed. The average of lattice constants, and the average of grain sizes increased with dopant from sample 1 to sample 4 (4.0512\AA , 4.2086\AA , 5.087\AA , and 5.1955\AA), (29.3nm, 32.4nm, 36.15 nm, and 37.98 nm) respectively, and they decreased with contents of Mg and Mn in sample 5 (5.0184\AA), (37.5 nm) respectively. Also the intensity increased with dopant of Mg and Mn in samples 1, 2, 3, and 5, and it decreased in sample 4.

The FTIR absorption spectroscopy has been used as a method to monitoring the formation of the Perovskite phase. The infrared spectra of the powders were collected in order to check the formation of $Ba_{(1-x)}Mg_xTi_{(1-x)}Mn_xO_3$, where $x=0.01, 0.2, 0.03, 0.4$, and $0, 05$ single perovskite. The FTIR absorption spectra of all samples showed that the transmittance decreased with contents of Mg and Mn.

The results of UV-visible spectra for indicate that the samples have a high absorbance in (0.189, 0.340, 0.346, 0.355, and .0910 a.u), and the optical band gap energy increased with dopant of Mg and Mn (3.18, 4.31, 4.35, 4.39, and 4.43 eV) respectively. Also, the reflective index of all samples decreased with doping of Mg and Mn (2.31, 2.10, 2.09, 2.089, and 2.083) respectively. The prepared material closed to insulator material because the results of optical band gap increased with dopant of Mg and Mn at $BaTiO_3$.

5.2. Recommendation:

1-Study the electrical and magnetic properties of $Ba_{(1-x)}Mg_xTi_{(1-x)}Mn_xO_3$, where $X=0.01, 0.2, 0.03, 0.4$, and $0, 05$

5.3.References:

- AAL, A. A., HAMMAD, T., ZAWRAH, M., BATTISHA, I. & HAMMAD, A. A. 2014. FTIR Study of Nanostructure Perovskite BaTiO₃ Doped with Both Fe³⁺ and Ni²⁺ Ions Prepared by Sol Gel Technique. *Acta Physica Polonica A*, 126, 1318-1321.
- Alaraj.B.,Mohammed,L.,& Mohammed.M .2017.Study the electrical properties of calcium-doped barium titanate ceramics.*Basic Science Series* , 38 ISSN: 2079-3057.
- Alaraj.B.,Mohammed,L.,& Mohammed.M .2017.Study the electrical properties of tin-doped barium titanate ceramics.*Basic Science Series* , 38 ISSN: 2079-3057.
- BADAPANDA, T., PARIDA, S. & ROUT, S. 2016. Structural and optical properties of dysprosium doped barium zirconium titanate ceramic. *Materials Letters*, 185, 415-419.
- AL-Jumaili ,S, Hamid & AL-Rawi , Ahmed ,Kh.2011. Effect of thermal annealing and laser radiation on the optical properties of AgAlS₂ thin films. *Iraqi Journal of Physics*,9, 16, PP. 79-83.
- BHALLA, A., GUO, R. & ROY, R. 2000. The perovskite structure—a review of its role in ceramic science and technology. *Materials Research Innovations*, 4, 3-26.
- BOBADE, S., GULWADE, D., KULKARNI, A. & GOPALAN, P. 2005. Dielectric properties of A-and B-site-doped BaTiO₃ (I): La-and Al-doped solid solutions. *Journal of applied physics*, 97, 074105.
- CAI, W., FU, C., GAO, J. & ZHAO, C. 2011. Dielectric properties and microstructure of Mg doped barium titanate ceramics. *Advances in Applied Ceramics*, 110, 181-185.
- CHOUDHURY, S., AKTER, S., RAHMAN, M., BHUIYAN, A., RAHMAN, S., KHATUN, N. & HOSSAIN, M. 2008. Structural, dielectric and electrical properties of zirconium doped barium titanate perovskite. *Journal of Bangladesh Academy of Sciences*, 32.
- CUI, B., YU, P., TIAN, J. & CHANG, Z. 2006. Preparation and characterization of Co-doped BaTiO₃ nanosized powders and ceramics. *Materials Science and Engineering: B*, 133, 205-208.
- DAS, S., ROUT, P., PRADHAN, S. & ROUL, B. 2012. Effect of equiproportional substitution of Zn and Mn in BaTiO₃ ceramic—An index to multiferroic applications. *Journal of Advanced Ceramics*, 1, 241-248.
- EMRE, F. Bilge., SAYILKAN Funda, & SIMSEK Can .2014. SYNTHESIS AND CHARACTERIZATION OF NANO-BaTiO₃ POWDER BY A HYDROTHERMAL METHOD. *International Journal of Latest Research in Science and Technology*,3, ISSN (Online):2278-5299.
- ESWARAMOORTHY, V., SEBASTIAN, S. & WILLIAMS, R. V. 2015. Influence of Ga doping on the structural, optical and electrical properties of Ba_{0.6}Sr_{0.4}TiO₃ thin films. *Int. J. Sci. Technol. Res*, 4, 86-91.
- GARCÍA-HERNÁNDEZ, M., CHADEYRON, G., BOYER, D., GARCÍA-MURILLO, A., CARRILLO-ROMO, F. & MAHIOU, R. 2013. Hydrothermal synthesis and characterization of europium-doped barium titanate nanocrystallites. *Nano-Micro Letters*, 5, 57-65.
- GATTU, S., PRASADU, V. D. & RAMESH, K. V. 2015. Effect of Zr on Structural and Dielectrical Properties of (Ba_{0.9}Mg_{1.0})(Zr_xTi_{1-x})O₃ Ceramics. *Advances in Materials Physics and Chemistry*, 5, 419.

- HAO, S., FU, D., LI, J., WANG, W. & SHEN, B. 2011. Preparation and characterization of Ag-doped BaTiO₃ conductive powders. *International Journal of Inorganic Chemistry*, 2011.
- HERNÁNDEZ LARA, J. P., PEREZ LABRA, M., BARRIENTOS HERNÁNDEZ, F. R., ROMERO SERRANO, J. A., ÁVILA DÁVILA, E. O., THANGARASU, P. & HERNÁNDEZ RAMIREZ, A. 2017. Structural Evolution and Electrical Properties of BaTiO₃ Doped with Gd³⁺. *Materials Research*, 20, 538-542.
- IMAM, A. T. A. 2017. Synthesis and Characterization of New double Perovskite X₂YVO₆ (X= Mg, Ca and Sr). Al-Neelain University.
- JENKINS, R. 2000. X-Ray Techniques: Overview. *Encyclopedia of analytical chemistry*.
- JOHANSSON, M. & LEMMENS, P. 2007. Crystallography and chemistry of perovskites. *Handbook of magnetism and advanced magnetic materials*.
- KADIRA, L., ELMESBAHI, A. & SAYOURI, S. 2016. Dielectric study of calcium doped barium titanate Ba_{1-x}Ca_xTiO₃ ceramics. *International Journal of Physical Sciences*, 11, 71-79.
- KAUR, A., SINGH, A., SINGH, L., MISHRA, S., BABU, P., ASOKAN, K., KUMAR, S., CHEN, C., YANG, K. & WEI, D. 2016. Structural, magnetic and electronic properties of iron doped barium strontium titanate. *RSC Advances*, 6, 112363-112369.
- KHARE, A. & CHAUHAN, N. 2015. The effect of Mg doping on structural and luminescent properties of Barium Strontium Titanate (BST). *Physics Procedia*, 76, 86-91.
- KHONGNAKHON, T. & JONGPRATEEP, O. Ba_{0.9}A_{0.1}TiO₃ (A= Al and Mg) Powders Synthesized by Solid State Reaction Technique and their Dielectric Properties. *Advanced Materials Research*, 2013. *Trans Tech Publ*, 603-606.
- Korman, I., Alaya, M. N. & Al-Okla, M. 2011. Study of some of the physiochemical properties of the oxide Mn₂O₃/MgO. *Basic Science Serise*, 78, ISS: 2227-9210.
- LANGHAMMER, H., MULLER, T., FELGNER, K.-H. & ABICHT, H.-P. 2000a. Influence of strontium on manganese-doped barium titanate ceramics. *materials Letters*, 42, 21-24.
- LANGHAMMER, H. T., MULLER, T., FELGNER, K. H. & ABICHT, H. P. 2000b. Crystal Structure and Related Properties of Manganese-Doped Barium Titanate Ceramics. *Journal of the American Ceramic Society*, 83, 605-611.
- LI, W., XU, Z., CHU, R., FU, P. & ZANG, G. 2010. Piezoelectric and Dielectric Properties of (Ba_{1-x}Ca_x)(Ti_{0.95}Zr_{0.05})O₃ Lead-Free Ceramics. *Journal of the American Ceramic Society*, 93, 2942-2944.
- L. Wu, M-C. Chure, K-K. Wu, W-C. Chang, M-J. Yang, W-K. Liu, and M-J. Wu. 2009. Dielectric properties of barium titanate ceramics with different materials powder size, *Ceramics International*, 35 (2009) 957- 960.
- MICLEA, C., TANASOIU, C., MICLEA, C. F. & GHEORGHIU, A. Structural, electrical and dielectric properties of uranium doped barium titanate. *Materials science forum*, 2006. *Trans Tech Publ*, 1269-1273.
- MOHAMED, S. & DUGHAIISH, Z. 2012. Microstructural and optical investigations of Ce-doped barium titanate thin films by FTIR and spectroscopic ellipsometry. *Philosophical Magazine*, 92, 1212-1222.
- MORRISON, F. D., SINCLAIR, D. C. & WEST, A. R. 1999. Electrical and structural characteristics of lanthanum-doped barium titanate ceramics. *Journal of Applied Physics*, 86, 6355-6366.

- OWEN, A. 1996. Fundamentals of UV-visible spectroscopy.
- PARKASH, O., KUMAR, D., DWIVEDI, R., SRIVASTAVA, K., SINGH, P. & SINGH, S. 2007. Effect of simultaneous substitution of La and Mn on dielectric behavior of barium titanate ceramic. *Journal of materials science*, 42, 5490-5496.
- PAVIA, D. L., LAMPMAN, G. M., KRIZ, G. S. & VYVYAN, J. A. 2008. Introduction to spectroscopy, Cengage Learning.
- PETRARU, A. I. 2003. Optical and electro-optical properties of BaTiO₃ thin films and Mach-Zehnder waveguide modulators.
- REICHENBÄCHER, M. & POPP, J. 2012. Challenges in molecular structure determination, Springer Science & Business Media.
- SENGODAN, R., CHANDAR SHEKAR, B. & SATHISH, S. 2012. Synthesis and characterization of BaTiO₃ nano particles by organic precursor method. *IJMER*, 2, 043-045.
- SIMON M. SZE, KWOK. N. 2006. Physics of semiconductors Devices. 3, ISBN:978-0471.
- SIMONESCU, C. M. 2012. Application of FTIR spectroscopy in environmental studies. *Advanced Aspects of Spectroscopy*. InTech.
- STOJANOVIĆ, B., MASTELARO, V., PAIVA, S. C. & VARELA, J. A. 2004. Structure study of donor doped barium titanate prepared from citrate solutions. *Science of Sintering*, 36, 179-188.
- SU, B. & BUTTON, T. 2004. Microstructure and dielectric properties of Mg-doped barium strontium titanate ceramics. *Journal of Applied Physics*, 95, 1382-1385.
- TANAKA, T. 1954. Barium titanate ceramics and their applications.
- TILLEY, R. J. 2016. Perovskites: structure-property relationships, John Wiley & Sons.
- TING, C. J., PENG, C. J., LU, H. Y. & WU, S. T. 1990. Lanthanum-Magnesium and Lanthanum-Manganese Donor-Acceptor-Codoped Semiconducting Barium Titanate. *Journal of the American Ceramic Society*, 73, 329-334.
- VIJATOVIĆ, M., BOBIĆ, J. & STOJANOVIĆ, B. 2008. History and challenges of barium titanate: Part I. *Science of Sintering*, 40, 155-165.
- WAHL, R., VOGTENHUBER, D. & KRESSE, G. 2008. SrTiO₃ and BaTiO₃ revisited using the projector augmented wave method: Performance of hybrid and semilocal functionals. *Physical Review B*, 78, 104116.
- WANG, M. J., ZHANG, Q. L., ZHAO, X. H. & YANG, H. Dielectric Properties and Microstructure of Y-Al-Ga-Si Co-Doped Barium Titanate Ceramics. *Key Engineering Materials*, 2014. Trans Tech Publ, 700-704.
- WANG, S., ZHANG, S., ZHOU, X., LI, B. & CHEN, Z. 2005. Effect of sintering atmospheres on the microstructure and dielectric properties of Yb/Mg co-doped BaTiO₃ ceramics. *Materials Letters*, 59, 2457-2460.
- WANG, S., ZHANG, S., ZHOU, X., LI, B. & CHEN, Z. 2006. Investigation on dielectric properties of BaTiO₃ co-doped with Ni and Nb. *Materials Letters*, 60, 909-911.
- YASMIN, S., CHOUDHURY, S., HAKIM, M., BHUIYAN, A. & RAHMAN, M. 2011. Structural and dielectric properties of pure and cerium doped barium titanate. *Journal of Ceramic Processing Research*, 12, 387-391.
- ZHU, H., GUO, Z., YANG, W.-D., CHANG, W.-F. & WANG, C.-C. 2011. Preparation and characterization of nanometer-sized (Pb_{1-x}, Ba_x) TiO₃

powders using acetylacetone as a chelating agent in a non-aqueous sol-gel process. *Ceramics International*, 37, 3203-3209.

ZHU, L. F., ZHANG, B. P., ZHAO, X. K., ZHAO, L., ZHOU, P. F. & LI, J. F. 2013. Enhanced Piezoelectric Properties of $(\text{Ba}_{1-x}\text{Ca}_x)(\text{Ti}_{0.92}\text{Sn}_{0.08})\text{O}_3$ Lead-Free Ceramics. *Journal of the American Ceramic Society*, 96, 241-245.

